ISSN 2531-2189

Volume 5, Issue 15 – January – June – 2021

Journal of Mechanical Engineering

ECORFAN®

Journal of Mechanical Engineering, Volume 5, Number 15, June - 2021, is a biannually Journal edited by ECORFAN-Spain. Matacerquillas Street 38, CP: 28411. Moralzarzal - Madrid. WEB: http://www.ecorfan.org/spain/rj_ingenieria_mec.php, revista@ecorfan.org. Editor in Chief: SERRUDO-GONZALES, Javier, BsC. ISSN 2531-2189. Responsible for the last update of this issue ECORFAN Computer Unit. Imelda Escamilla Bouchán, PhD. Vladimir Luna Soto, PhD. Updated as of June 30, 2021.

Journal of Mechanical Engineering

Definition of Journal

Scientific Objectives

Support the International Scientific Community in its written production of Science, Innovation Technology in the Area of Engineering and Technology, in the Subdisciplines of pumps and equipment for handling liquids, bearings, air compressors, gears, refrigeration equipment, mechanical power transmission equipment, pneumatic equipment, equipment and industrial machinery, agricultural machinery, oil extraction machinery, printing and reproduction machinery , Mining Machinery, Hydraulic Machinery, Specialized Industrial Machinery, Nuclear Machinery, Paper Manufacturing Machinery, Machinery for the Food Industry, Material Handling Machinery, Textile Machinery, Steam Machinery, Vending and Distributor Machines, Machines, Tools and Accessories, Heating Material, Construction Material, Dies, Insoles and Gauges, Internal Combustion Engines (General), Gas Engines, Machined Operations.

ECORFAN-Mexico SC is a Scientific and Technological Company in contribution to the Human Resource training focused on the continuity in the critical analysis of International Research and is attached to CONACYT-RENIECYT number 1702902, its commitment is to disseminate research and contributions of the International Scientific Community, academic institutions, agencies and entities of the public and private sectors and contribute to the linking of researchers who carry out scientific activities, technological developments and training of specialized human resources with governments, companies and social organizations.

Encourage the interlocution of the International Scientific Community with other Study Centers in Mexico and abroad and promote a wide incorporation of academics, specialists and researchers to the publication in Science Structures of Autonomous Universities - State Public Universities - Federal IES - Polytechnic Universities - Technological Universities - Federal Technological Institutes - Normal Schools - Decentralized Technological Institutes - Intercultural Universities - S & T Councils - CONACYT Research Centers.

Scope, Coverage and Audience

Journal of Mechanical Engineering is a Journal edited by ECORFAN-México S.C in its Holding with repository in Spain, is a scientific publication arbitrated and indexed on a quarterly basis. It supports a wide range of contents that are evaluated by academic pairs by the Double-Blind method, around topics related to the theory and practice of pumps and equipment for handling liquids, bearings, air compressors, gears, cooling equipment, mechanical power transmission equipment, pneumatic equipment, equipment and industrial machinery, agricultural machinery, oil extraction machinery , printing and reproduction machinery, mining machinery, hydraulic machinery, specialized industrial machinery, nuclear machinery, paper manufacturing machinery, machinery for the food industry, material handling machinery, textile machinery, steam machinery, vending machines and distributors, machines, tools and accessories, heating material, building material, dies, insoles and gauges, internal (general) combustion engines, gas engines , mechanized operations with diverse approaches and perspectives, which contribute to the dissemination of the development of Science Technology and Innovation that allow arguments related to decision-making and influence the formulation of international policies in the Field of Engineering and Technology Sciences. The editorial horizon of ECORFAN-Mexico® extends beyond the academy and integrates other research and analysis segments outside this field, as long as they meet the requirements of argumentative and scientific rigor, as well as addressing topics of general and current interest of the International Scientific Society.

Editorial Board

Arbitration Committee

Assignment of Rights

The sending of an Article to Journal of Mechanical Engineering emanates the commitment of the author not to submit it simultaneously to the consideration of other series publications for it must complement the Originality Format for its Article.

The authors sign the Authorization Format for their Article to be disseminated by means that ECORFAN-Mexico, S.C. In its Holding Spain considers pertinent for disclosure and diffusion of its Article its Rights of Work.

Declaration of Authorship

Indicate the Name of Author and Coauthors at most in the participation of the Article and indicate in extensive the Institutional Affiliation indicating the Department.

Identify the Name of Author and Coauthors at most with the CVU Scholarship Number-PNPC or SNI-CONACYT- Indicating the Researcher Level and their Google Scholar Profile to verify their Citation Level and H index.

Identify the Name of Author and Coauthors at most in the Science and Technology Profiles widely accepted by the International Scientific Community ORC ID - Researcher ID Thomson - arXiv Author ID - PubMed Author ID - Open ID respectively.

Indicate the contact for correspondence to the Author (Mail and Telephone) and indicate the Researcher who contributes as the first Author of the Article.

Plagiarism Detection

All Articles will be tested by plagiarism software PLAGSCAN if a plagiarism level is detected Positive will not be sent to arbitration and will be rescinded of the reception of the Article notifying the Authors responsible, claiming that academic plagiarism is criminalized in the Penal Code.

Arbitration Process

All Articles will be evaluated by academic peers by the Double Blind method, the Arbitration Approval is a requirement for the Editorial Board to make a final decision that will be final in all cases. MARVID® is a derivative brand of ECORFAN® specialized in providing the expert evaluators all of them with Doctorate degree and distinction of International Researchers in the respective Councils of Science and Technology the counterpart of CONACYT for the chapters of America-Europe-Asia- Africa and Oceania. The identification of the authorship should only appear on a first removable page, in order to ensure that the Arbitration process is anonymous and covers the following stages: Identification of the Journal with its author occupation rate - Identification of Authors and Coauthors - Detection of plagiarism PLAGSCAN - Review of Formats of Authorization and Originality-Allocation to the Editorial Board-Allocation of the pair of Expert Arbitrators-Notification of Arbitration -Declaration of observations to the Author-Verification of Article Modified for Editing-Publication.

Instructions for Scientific, Technological and Innovation Publication

Knowledge Area

Work should be unpublished and refer to issues of Pumps and equipment for handling liquids, bearings, air compressors, gears, cooling equipment, mechanical power transmission equipment, pneumatic equipment, equipment and industrial machinery, agricultural machinery, oil extraction machinery, printing and reproduction machinery, mining machinery, hydraulic machinery, specialized industrial machinery, nuclear machinery, machinery to manufacture paper , machinery for the food industry, material handling machinery, textile machinery, steam machinery, vending machines and distributors, machines, tools and accessories, heating material, building material, dies, insoles and gauges, internal combustion engines (general), gas engines, machined operations and other topics related to engineering and technology sciences.

Presentation of Content

In volume five, issue fifteen, as the first article we present, *Failure in a pipe due to defective maintenance*, by SALGADO-LÓPEZ, Juan Manuel, OJEDA-ELIZARRARAS, José Luis, LOPEZ-MONROY, Francisco Ignacio and TELLO-RICO, Mauricio, with secondment at the CIDESI, as a second article we present, *Effect of induction heating on Vickers and Knoop hardness of 1045 steel heat treated*, by MARTÍNEZ-VÁZQUEZ, J. Merced, RODRÍGUEZ-ORTIZ, Gabriel, HORTELANO-CAPETILLO, J. Gregorio and PÉREZ-PÉREZ, Arnulfo, with an appointment at Universidad Politécnica de Juventino Rosas, as a third article we present, *The numerical characterization of the gas turbine blade with static stress analysis applying finite element method*, by VILLAGRÁN-VILLEGAS, Luz Yazmín, HERNÁNDEZ-GÓMEZ, Luis Héctor, MARTÍNEZ-CRUZ, Miguel Ángel and ROJAS-RAMÍREZ, Jorge Armando, with secondment at the Instituto Politécnico Nacional and Universidad de Veracruz, as fourth article we present, *Vibration analysis in a rotodynamic system*, by GAMBOA-MARTÍN, Vianney Aurora, RODRIGUEZ-BLANCO, Marco Antonio, DURÁN-MORALES, Iván and MARTÍNEZ-RODRÍGUEZ, Gilberto, with secondment Universidad Autónoma del Carmen.

Content

Article **Journal of Mechanical Engineering**
June 2021, Vol.5 No.15 1-7

Failure in a pipe due to defective maintenance

Falla de tubería por deficiencias en mantenimiento

SALGADO-LÓPEZ, Juan Manuel†*, OJEDA-ELIZARRARAS, José Luis, LOPEZ-MONROY, Francisco Ignacio and TELLO-RICO, Mauricio

CIDESI, Materials Technology, Metallography Laboratory and Failure Analysis. Mexico.
CIDESI, Joining Technologies, Welding Laboratory, Mexico.

ID 1st Author: *Juan Manuel, Salgado-Lopez* / **ORC ID:** 0000-0002-2384-1887, **CVU CONACYT ID:** 94744

ID 1st Co-author: *José Luis, Ojeda-Elizarrarás* / **ORC ID:** 0000-0001-8412-7778, **CVU CONACYT ID:** 81630

ID 2nd Co-author: *Abraham, Silva-Hernandez* / **ORC ID:** 0000-0003-2699-8107, **CVU CONACYT ID:** 726099

ID 3rd Co-author: *Jesús Mauricio, Tello-Rico* / **ORC ID:** 0000-0002-5657-2134, **CVU CONACYT ID:** 586320

DOI: 10.35429/JME.2021.15.5.1.7 Received January 10, 2021; Accepted June 30, 2021

Abstract

Proper maintenance of energy transport pipelines is a part of energy efficiency since energy losses during transport are reduced with good maintenance practices as well as the mechanical integrity can be known. Moreover, it reduces the risk of accidents or environmental damage. This work is an example of the experiences that must be taken into account for optimal pipeline maintenance and consisted of a failure analysis performed on a 20-inch diameter "T" connection, which plays an important role in the energy transportation process and it was found to be partially buried with exposure to rainwater. Preventive maintenance consists of visual inspection, cleaning, and coating with paint. The results indicated that the failure begun due to fatigue with origin in weld defects and the fracture grew up due to an overload, which caused the crack to grow following the region of the material with loss of thickness induced by corrosion pitting.

Failure, Corrosion, Defective maintenance

Resumen

El mantenimiento adecuado de los ductos para transporte de energéticos es parte de la eficiencia energética, ya que así se logran reducir las pérdidas durante el transporte y se puede conocer la integridad mecánica de estos y con ello reducir el riesgo de accidentes o daños ambientales. Este trabajo es un ejemplo de las experiencias que deben ser tomadas en cuenta para un mantenimiento óptimo de los ductos y consistió de un análisis de falla realizado en una conexión tipo “T” de 20 pulgadas de diámetro, la cual tiene un papel importante en el proceso de transporte de energéticos y que se encontraba enterrado parcialmente con exposición al agua pluvial. El mantenimiento preventivo consistía de inspección visual, limpieza y recubrimiento con pintura. Los resultados indican que la falla ocurrió por fatiga iniciada en defectos de soldadura y la fractura termino por una sobrecarga que dio lugar a que la grieta creciera siguiendo la región del material con pérdida de espesor inducida por picaduras por corrosión.

Falla, Corrosión, Mantenimiento

Citation: SALGADO-LÓPEZ, Juan Manuel, OJEDA-ELIZARRARAS, José Luis, LOPEZ-MONROY, Francisco Ignacio and TELLO-RICO, Mauricio. Failure in a pipe due to defective maintenance. Journal of Mechanical Engineering. 2021. 5-15:1-7.

* Correspondence to the Author (Email: msalgado@cidesi.edu.mx)
† Researcher contributing as first author.

Introduction

Preventive maintenance is crucial for well-functioning of industry and to avoid accidents.

This is especially true for energy industry because there are risks of accidents or leaks, which jeopardizes the health of people and the environment Nevertheless, in some cases preventive maintenance consists only on external cleaning. This bad practice leads to consequences as the shown in this work.

Loss of productivity due to unplanned maintenance or repairs are some of the mild consequences of such shallow maintenance. Besides temporary repairs require additional work for their final correction, or in the worst case, they fail before being corrected. All of this commonly leads to a worst situation.

When a failure occurs, which affects production, the quality of the products, the safety of people or that might cause a serious environmental impact; it is essential to carry out a failure analysis to determine the metallurgical cause that led to the failure. From the conclusions of the analysis, real actions can be undertaken in order to prevent such events from occurring again. Failure analysis, it is linked to the criticality of the energy production or transport equipment to prioritize preventive maintenance activities and their planning; since maintenance requires studying the incidents that happened and providing real solutions to avoid them.

This work consisted of a failure analysis performed on a 20-inch diameter “T” type connection, which plays an important role in the energy transport process. The objective of this work was to determine the metallurgical mechanism, which led to the fracture of this component and with this work it is shown that a poor practice in preventive maintenance leads to process failures and unplanned stoppages.

Methodology

The construction of this “T” type connection dated from 1980 and the material was ASTM A 53 grade B steel. This component was approximately 2.30 meters long, 500 millimeters in diameter and approximately 7.85 millimeters thickness.

It should be mentioned that the thickness was not constant since the specimen under study showed red oxidation on both sides; the “T” connection was 500 millimeters in diameter, in addition to a 300 millimeters of diameter hole. There was a primary crack that began transversely to the radius of the tube and then towards a semicircle of approximately 50 centimeters long whose possible origin was detected in the joint weld of the "T" with the tube. This is shown in figure 1.

In order to achieve the aim of this work, the following techniques were applied: visual inspection with the naked eye and using Leica brand stereographic microscope, this technique was carried out to demonstrate the circumstance of delivery to the laboratory of the specimen under study and determine the origin of the fracture if there is significant macroscopic evidence.

Figure 1 The image the connection type "T" in the condition of delivery to the laboratory. Note the fracture and coating on the external surface
Source: Own work

The thickness measurement was done by means of the ultrasonic testing with a straight beam receiver using a GE equipment model USM / DMS Go, this non-destructive testing was necessary in order to be able to determine the areas of the “T” connection with reduction in thickness.

To find damage in the microstructure of this component steel, a microstructural analysis was carried out using a Nikon Epiphot 440 brand metallographic optical microscope. The samples were taken by transversal mechanical cuts. These samples were mounted on Bakelite, grinded and polished using sandpaper from 120 to 2000. After that these samples were polished using 1 micron particle size alumina powder and subsequently etched with nital 2 to reveal the microstructure.

ISSN-2531-2189

Finally, the fracture pattern of the failed "T" connection was observed by a Phillips Model XL-30 scanning electron microscope (SEM) and EDS elemental microanalysis with EDAX.

Results

Visual testing on the "T" type connection showed that the pattern of the crack at the ends was ductile and that the origin was located in the weld toe of the "T" connection (figure 2). From this fact it can be deduced that the origin of the crack was located at the weld toe and that the fracture was initiated by some defect in it.

Figure 2 The image shows the fracture zone in the region of the weld
Source: Own work

Moreover, it should be mentioned that by this technique, corrosion pitting was found in the area near the crack (figure 3). Figure 3 shows that the crack grew following the regions of the material with reduction in thickness due to corrosion, since the crack changed its path respecting to the origin located at the weld toe.

Figure 3 The image shows the right area of the crack. There is seen the change in crack growth from the weld toe to the body of the pipe
Source: Own work

Visual testing of the fracture surface showed an incomplete fusion and a layer of red corrosion products. This evidence is shown in Figures 4. With this evidence it is verified that the welding defects played a role in the crack growth of this component.

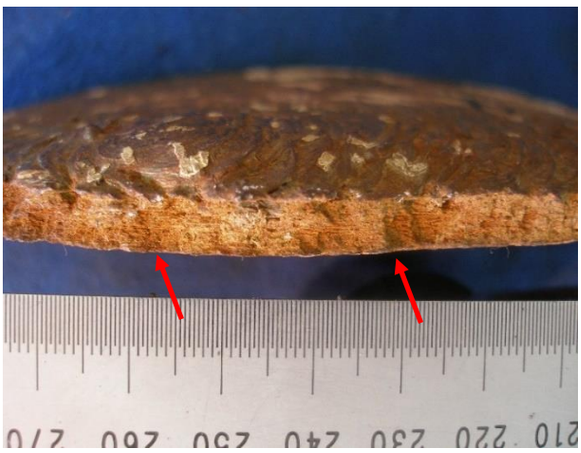

Figure 4 The image shows the fracture surface. The fracture surface is covered with a layer of red corrosion products and there is seen a lack of fusion
Source: Own work

In the same way, visual testing also revealed the existence of red corrosion products inside the "T" connection, which indicates that there was oxygen corrosion in this part of the component. This resulted in a loss of thickness. Figure 5 shows evidence of corrosion pitting inside the "T" connection.

On the other hand, the thickness measurement carried out on the connection type "T" revealed that there is only a slight reduction in thickness in the area of the fracture with respect to the main tube of the connection "T". This is shown in tables 1 and 2.

Figure 6 shows the regions where the thicknesses were measured with the straight beam ultrasonic testing.

ISSN-2531-2189

Figure 5 The image shows corrosion pitting inside the tube. (The layer of red corrosion products was removed from the surface)
Source: Own work

Figure 6 The image shows the regions where the thicknesses measurements were carried out
Source: Own work

From Tables 1 and 2 it can be noted that the maximum thickness of the main tube was 5.92 millimeters; while the minimum thickness detected was 5.31 millimeters and this was in the pitted area (close to the fracture surface). Perhaps this data does not seem relevant but if this reduction in thickness in this area of "T" the component is combined with the welding defects found by visual inspection, we can deduce that the stress applied by the internal pressure of the tube in this region of the connection was more higher than in other regions of the same specimen.

Measurement points in the HAZ							
	1	2	3	4	5	6	7
A	5.41	5.44	5.53	5.64	5.59	5.31	5.36

Table 1 Results of thickness measurements in the HAZ
Source: Own work

Measurement points (pipe).											
	1	2	3	4	5	6	7	8	9	10	11
A	5,72	5.59	5.72	5.74	5.82	5.82	5.84	5.84	…	5.82	5.89
B	5.74	5.74	5.72	5.74	5.79	5.79	5.79	5.82	5.89	5.84	5.89
C	5.79	5.79	5.66	5.79	5.77	5.79	5.79	5.77	5.79	5.79	5.66
D	5.61	5.59	5.56	5.54	5.59	5.77	5.59	5.77	5.84	5.87	5.88
E	5.74	…	…	5.82	5.77	5.74	5.82	5.69	5.79	5.74	5.77
F	5.77	…	…	5.69	5.79	5.84	5.77	5.61	5.79	5.79	5.89
G	5.82	…	….	5.82	5.84	5.84	5.84	5.84	5.84	5.84	5.92

Table 2 Results of thickness measurements along the "T" connection
Source: Own work

The metallographic analysis carried out in different regions of the "T" connection showed evidence that defects such as: trapped slag or lack of fusion, which serve as stress risers. This is shown in figure 7.

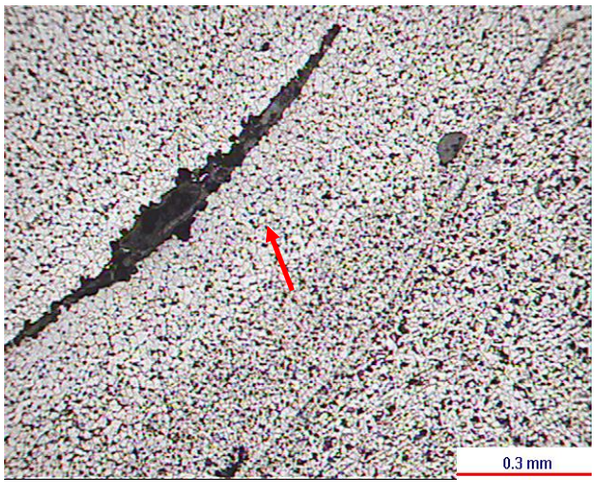

Figure 7 Microstructure of the welded joint. Incomplete fusion is observed
Source: Own work

Similarly, the cross-sectional micrograph at the weld joint showed evidence of a fold on the outside of the weld. This can be seen in Figure 8. Besides, metallographic analysis confirmed the presence of corrosion pitting within the tube material of the "T" connection in the fracture region of the specimen. This fact is very important since corrosion pitting is a very severe form of damage; because the bites act as stress concentrators. This can be seen in figure 9.

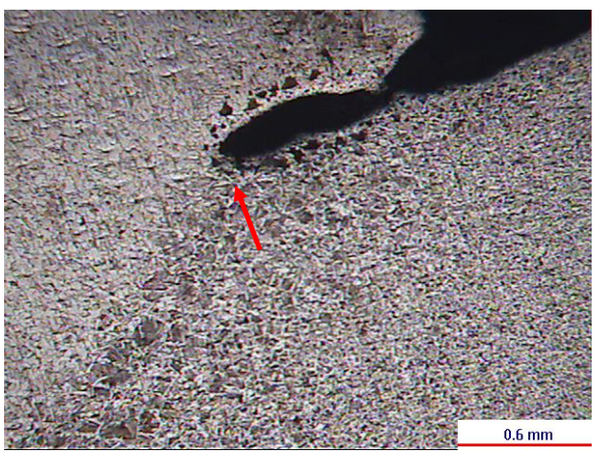

Figure 8 Microstructure in the fold of weld
Source: Own work

Figure 10 shows the microstructure in a cross section to the fracture surface of the "T" connection, there is evidence of corrosion pitting and a secondary crack that grows from the pit.

ISSN-2531-2189

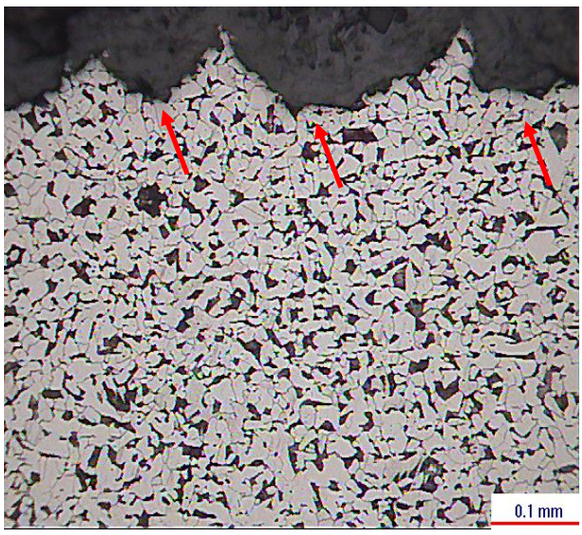

Figure 9 Micrograph at 200x. There is seen the microstructure of the base material and pitting on the outer surface of the base material
Source: Own work

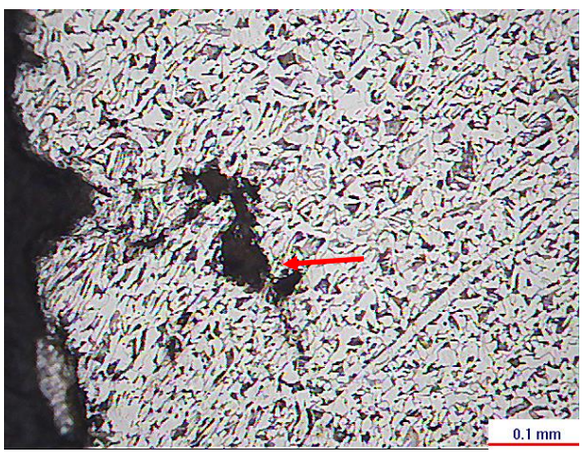

Figure 10 Micrograph at 200x. Microstructure near the crack
Source: Own work

The fractographic analysis showed beach marks near the origin of the crack. This means that the crack growth occurred due to fatigue (figure 11). However, it should be mentioned that the corrosion degraded the evidence. Furthermore, weld defects such as incomplete fusion and porosity were found in this region of the fracture. This fact shows that these defects are stress risers where fatigue cracks begun. This matches with the fact that this component works in compression cycles during oil / decompression transport.

On the other hand, in the area of the crack where it grew away from the weld toe, a wooden pattern was observed (figure 12). This pattern is the mixture between a cleavage and dimples.

This fact indicates that the crack grew from welding defects due to the fatigue mechanism and then it finished cracking due to an overload.

This overload was conjunction of the work stress of the connection acting in the region of the pipe with thickness reduction. This region that had to withstand the work effort was reduced in mechanical strength due to the reduction in thickness caused by corrosion pitting.

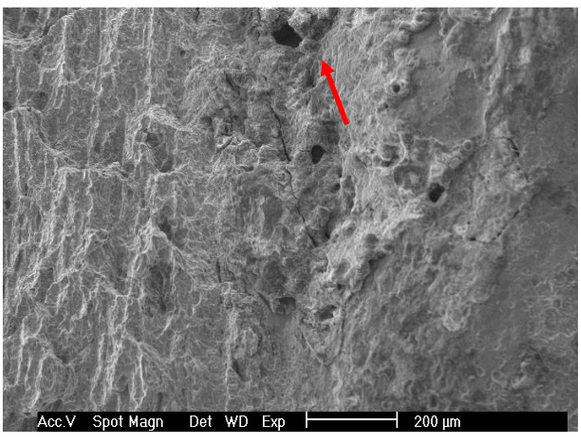

Figure 11 Fracture surface in the partial fusion zone. Incomplete fusion, porosity cavities and secondary cracks are observed
Source: Own work

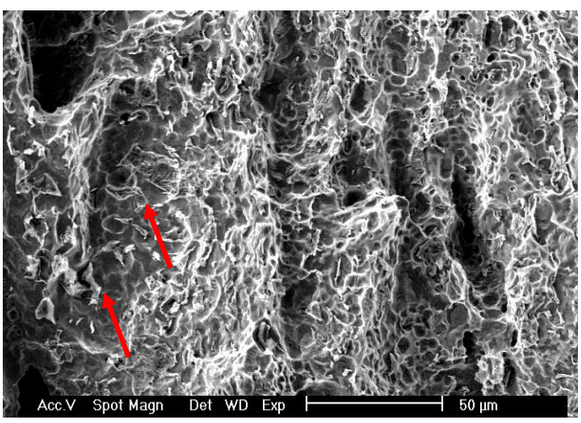

Figure 12 Fracture surface at the crack tip away from the welded joint. The image shows cleavage and dimples
Source: Own work

Discussion

Considering the above mentioned results, it can be said that the 20-inch diameter “T” type connection failed due to the metallurgical mechanism known as fatigue. This damage started due to defects in weld and the crack grew catastrophically due to an overload. It acted in the region with thickness reduction due to corrosion pitting.

ISSN-2531-2189

One has to consider that the failure of this component occurred despite preventive maintenance, which consisted of visual inspection and painting; then it can be deduced that this was not a good maintenance practice.

Then, from the evidence previously shown and discussed it is clear that at the beginning the crack grew by fatigue due to pressure/decompression cycles with origin in weld defects such as incomplete penetration. These types of welding defects are detected by non-destructive tests, this is also valid for the growth of the crack and the loss of thickness in the HAZ. Besides, the results of non-destructive testing can be used to feed a methodology of mechanical integrity, with which it is possible to give predictions of the growth of corrosion damage and thus design strategies for the replacement of said component.

Finally, combining the previously discussed evidences with the defective practice maintenance mentioned it can be deduced that good preventive maintenance practices could avoid the catastrophic failure of this component.

Acknowledgements

The authors wish to thank the CIDESI Metallography and Failure Analysis Laboratory for their support in carrying out this work.

Conclusions

The “T” type connection failed due to fatigue, which started in defects in the HAZ and the fracture grew catastrophically due to an overload acting in the region with a decrease in thickness due to corrosion pitting.

Weld defects act as crack initiators in equipment that is subjected to loading / unloading cycles and corrosion decreases the thickness of the material, causing cracks to grow in these places.

The evidence previously discussed shows that good preventive maintenance practices could prevent the catastrophic failure of this type of components.

References

Babu, S. K., & Natarajan, S. (2008). Influence of heat input on high temperature weldment corrosion in submerged arc welded power plant carbon steel. Materials & Design, 29(5), 1036-1042.

Barsom, J. M., & Pellegrino Jr, J. V. (2002). Failure analysis of welded steel moment-resisting frame connections. Journal of materials in civil engineering, 14(1), 24-34.

Bilmes, P. D., Llorente, C. L., Méndez, C. M., & Gervasi, C. A. (2009). Microstructure, heat treatment and pitting corrosion of 13CrNiMo plate and weld metals. Corrosion Science, 51(4), 876-881.

Chaves, I. A., & Melchers, R. E. (2011). Pitting corrosion in pipeline steel weld zones. Corrosion Science, 53(12), 4026-4032.

Cheng, B., Ye, X., Cao, X., Mbako, D. D., & Cao, Y. (2017). Experimental study on fatigue failure of rib-to-deck welded connections in orthotropic steel bridge decks. International Journal of Fatigue, 103, 157-167.

Davis, J. R. (Ed.). (2006). Corrosion of weldments. ASM international.

Lu, Y., Jing, H., Han, Y., & Xu, L. (2016). Effect of welding heat input on the corrosion resistance of carbon steel weld metal. Journal of Materials Engineering and Performance, 25(2), 565-576.

Mashiri, F. R., Zhao, X. L., & Grundy, P. (2004). Stress concentration factors and fatigue failure of welded T-connections in circular hollow sections under in-plane bending. International Journal of Structural Stability and Dynamics, 4(03), 403-422.

Mellor, B. G., Rainey, R. C. T., & Kirk, N. E. (1999). The static strength of end and T fillet weld connections. Materials & design, 20(4), 193-205.

Mohammadi, F., Eliyan, F. F., & Alfantazi, A. (2012). Corrosion of simulated weld HAZ of API X-80 pipeline steel. Corrosion science, 63, 323-333.

ISSN-2531-2189

Oosterhof, S. A., & Driver, R. G. (2011). Effects of connection geometry on block shear failure of welded lap plate connections. Journal of Constructional Steel Research, 67(3), 525-532.
Peköz, T., & McGuire, W. (1979). Welding of sheet steel.

Shirinzadeh-Dastgiri, M., Mohammadi, J., Behnamian, Y., Eghlimi, A., & Mostafaei, A. (2015). Metallurgical investigations and corrosion behavior of failed weld joint in AISI 1518 low carbon steel pipeline. Engineering Failure Analysis, 53, 78-96.

Xing, S., Dong, P., & Threstha, A. (2016). Analysis of fatigue failure mode transition in load-carrying fillet-welded connections. Marine Structures, 46, 102-126.

ISSN-2531-2189

SALGADO-LÓPEZ, Juan Manuel, OJEDA-ELIZARRARAS, José Luis, LOPEZ-MONROY, Francisco Ignacio and TELLO-RICO, Mauricio. Failure in a pipe due to defective maintenance. Journal of Mechanical Engineering. 2021

Article **Journal of Mechanical Engineering**
June 2021, Vol.5 No.15 8-15

Effect of induction heating on Vickers and Knoop hardness of 1045 steel heat treated

Efecto del calentamiento por inducción en la dureza Vickers y Knoop del acero 1045 tratado térmicamente

MARTÍNEZ-VÁZQUEZ, J. Merced†*, RODRÍGUEZ-ORTIZ, Gabriel, HORTELANO-CAPETILLO, J. Gregorio and PÉREZ-PÉREZ, Arnulfo

Universidad Politécnica de Juventino Rosas, Metallurgical Engineering. Hidalgo 102, Community of Valencia, Santa Cruz de Juventino Rosas, Gto. 38253. Mexico.

ID 1st Author: *J. Merced, Martínez-Vázquez* / **ORC ID:** 0000-0002-6230-3846, **CVU CONACYT ID:** 93450

ID 1st Co-author: *Gabriel, Rodríguez-Ortiz* / **ORC ID:** 0000-0002-3702-4853, **CVU CONACYT ID:** 48565

ID 2nd Co-author: *J. Gregorio, Hortelano-Capetillo* / **ORC ID:** 0000-0002-3702-4853, **CVU CONACYT ID:** 347496

ID 3rd Co-author: *Arnulfo, Pérez-Pérez* / **ORC ID:** 0000-0003-1267-2560, **CVU CONACYT ID:** 176434

DOI: 10.35429/JME.2021.15.5.8.15 Received January 15, 2021; Accepted June 30, 2021

Abstract

AISI 1045 steel is a steel of medium carbon, widely used in machinery, the automotive industry, and the food industry, among others. Therefore, to fulfill its purpose, it is necessary to improve its mechanical resistance, wear resistance and resistance to fatigue through different surface heat treatments. Variables such as heating time and hence speed affect the thickness of the hardened layer and the microstructural characteristics of the area affected by heat treatment. The inspection of the transformation of phases during the treatment and the thickness of the boundary layer is generated by determining the hardness of the material, whose procedure is subject to the ASTM E92-17 and E384-17standards, which establish the methodology to be followed. Therefore, the objective of this work is to quantify the effect of three heating times at 1123 K on the hardening of AISI 1045 steel and the regularity of the hardened layer to ensure its functionality as a component subjected to friction, in addition to developing a table of equivalences between the Knoop (HK), Vickers (HK) and Rockwell C (HRC) hardness scales.

Induction, Microhardness, Quenching

Resumen

El acero AISI 1045, es un acero de medio carbono ampliamente utilizado en maquinaria, industria automotriz, industria alimenticia, entre otras. Por lo que para cumplir con su propósito es necesario mejorar su resistencia mecánica, resistencia al desgaste y la resistencia a la fatiga mediante distintos tratamientos térmicos superficiales. Las variables, como el tiempo de calentamiento y, por ende, la velocidad afecta el espesor de la capa endurecida y las características microestructurales de la zona afectada por el tratamiento térmico. La inspección de la transformación de fases durante el tratamiento y el espesor de la capa limite se genera mediante la determinación de la dureza del material, cuyo procedimiento está supeditado al seguimiento de las normas ASTM E92-17 y E384-17, las cuales establecen la metodología a seguir. Por lo que el objetivo del presente trabajo es cuantificar el efecto de tres tiempos de calentamiento a 1123 K sobre el endurecimiento del acero AISI 1045 y la regularidad de la capa endurecida para asegurar su funcionalidad como componente sometido a fricción además de elaborar una Table de equivalencias entre las escalas de dureza Knoop (HK), Vickers (HK) y Rockwell C (HRC).

Inducción, Microdureza, Temple

Citation: MARTÍNEZ-VÁZQUEZ, J. Merced, RODRÍGUEZ-ORTIZ, Gabriel, HORTELANO-CAPETILLO, J. Gregorio and PÉREZ-PÉREZ, Arnulfo. Effect of induction heating on Vickers and Knoop hardness of 1045 steel heat treated. Journal of Mechanical Engineering. 2021. 5-15:8-15.

* Correspondence to the Author (Email: jmartinez_ptc@upjr.edu.mx)
† Researcher contributing as first author.

Introduction

The mechanical strength, wear resistance and fatigue resistance of medium carbon steels, such as SAE1045, can be improved by different surface heat treatments such as flame, laser and induction heating. Compared with other surface hardening methods, induction hardening shows favorable characteristics such as controlled heating depth, rapid heating, energy saving, and good reproducibility. The typical procedure for induction heating involves heating the component to the austenitizing temperature range and then rapidly cooling it until it is below the martensitic temperature (Ms). Conventional methods to determine the hardening of steels involve heating the samples in an oven for several minutes at an austenitizing temperature that depends on the carbon content of the steel [1]; according to ASTM A255, the process involves Jominy heating and tempering for the samples for 30 minutes. For steels with carbon contents above 0.37% by weight, the standard indicates an austenitizing temperature prior to hardening. The standard assumes that the steels will produce an ASTM 7 grain size. Some studies have shown an inverse relationship between austenitic grain size and hardening [2-4], which consider austenitic grain sizes in the 4-8 range.

With induction heating, the heating ratios are higher and the austenitizing times are much shorter leading to the possibility of incomplete dissolution of carbides in the austenite. Clarke et al. [5] studied the transformation kinetics of austenite and carbide dissolution in 5150 grade steels, finding that for the quenched and tempered structure all carbides were dissolved at heating rates of up to 900 ° C / s.

The time-temperature cycles that can be achieved in induction surface heating vary from one hardened part to another and depends on the initial size of the cross section and the required depth [6]. Austenitizing times can be less than 2 s and greater than 10 s depending on the part treated and the parameters of the equipment.

The main objective of this work is to examine the effects of three heating times at austenitic temperatures of 1123 K on the hardening of 1045 steel and the regularity of the hardened layer to ensure their functionality as components subjected to friction, for which they will be carried out.

ISSN-2531-2189

Vickers and Knoop hardness tests to compare the degree of hardness at the beginning and end of the treatment; Furthermore, it is important to mention that there is controversy in the margin of error between microhardness scales such as the Vickers (HV) and the Knoop (HK), which can generate errors when converting to the Rockwell C (HRC) scale. For this reason, the methodology will be implemented to carry out the conversion between scales correctly and avoiding said error in the block & wing part manufactured by forging, which carries an induction hardening heat treatment, whose minimum hardness limit is 59 HRC and a maximum of 63 HRC; Likewise, the induction heating time on the thickness of the hardened layer will be correlated with the hardness.

Methodology to be developed

The research was carried out on SAE1045 steel pieces shown in Figure 1, due to their application, said samples must have a hardened outer layer in order to increase their resistance to wear, so they were subjected to a heat treatment of induction hardening. in a GH Induction equipment model 2X100MS150 / S. The process consists of austenitizing the material at 1123 K; For this, the equipment operating conditions were 37 kW of power at a frequency of 15 KHz, and later the pieces were cooled in a 5% polymer solution at 28 ° C, the austenitizing times were 2.0, 2.2 and 2.4 s and a total cycle of 39 s / piece. Once the pieces were tempered, they were cut transversely (Figure 1b), the evaluation points shown in the Figure. 1c correspond to the critical areas of the piece, in which hardness values greater than 50 HRC are required. The pieces were cut in a Leco MX205M metallographic cutter, with cooling during cutting to avoid heating and possible microstructural transformation of the surface.

Figure 1 Induction Hardened 1045 Steel Automotive Part
Source: Own, Solidworks

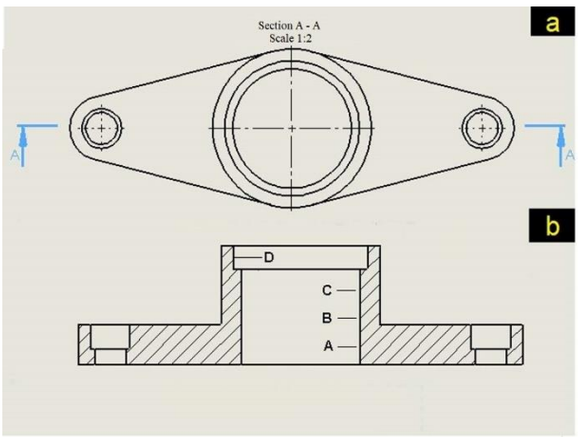

Figure 2 (a) Section studied and (b) points evaluated in the cut
Source: Own, Solidworks

After cutting, for the determination of the Vickers microhardness (HV), the samples were prepared metallographically, for this an intermediate roughing was carried out with abrasive paper of silicon carbide (SiC) grades 320, 400 and 600, then they were gave a fine slab with 800, 100, 1200 and 1500 grade abrasive paper; finally, the samples were polished with 9, 6 and 3 µm diamond paste. The microhardness tests were carried out with a Vickers Shidmazu HMV-G2 microdurometer, at a load of 0.5 kg and a load time of 10 s, 5 indentations were made per sample to obtain the statistical average and the standard deviation of the value of microhardness. The indentations were made every 100 µm in an area no greater than 1.5 mm; the foregoing in compliance with the ISO 6507-1 [7] and JIS Z2244 [8] standards, which regulate the determination of the effective depth of hardening. In addition to the microhardness tests, the Jominy curves were simulated using thermodynamic simulation software in order to predict the correlation between surface hardening and austenitic grain size.

Results

Optical microscopy of 1045 steel and nominal composition

The base material for the manufacture of the pieces is an AISI 1045 C-Mn steel whose typical composition is Fe-0.47, C-0.607, Mn-0.012, P-0.006, S-0.235, and Si-0.006, the values are given in percent by weight.

The microstructure of the analyzed AISI-1045 steel sample without heat treatment was composed of 88% pearlite (α + Fe3C) and 12% allotriomorphic ferrite (α), forming the first austenite grains. The microstructure of the material is shown in Figure 3.

Figure 3 Micrograph of the microstructure of AISI 1045 steel without heat treatment. Allotriomorphic ferrite is the light phase that describes the previous austenite grain boundaries, and pearlite is the darkest phase
Source: Own, Leco MX205M Microscope

Figure 4 shows the microstructures of the AISI-1045 steel samples heat-treated with induction heating at times of 2.0, 2.2 and 2.4 s at 1123 K, the images were acquired from the outermost area of the layer affected by the treatment. The microstructure, in the three conditions studied, showed the formation of martensite with plate and slat configurations. However, it can be observed at the lowest time studied, of 2.0 s, the presence of undissolved carbides due to the small size of austenitic grain, as has been reported in the literature (Figure 3a).

ISSN-2531-2189

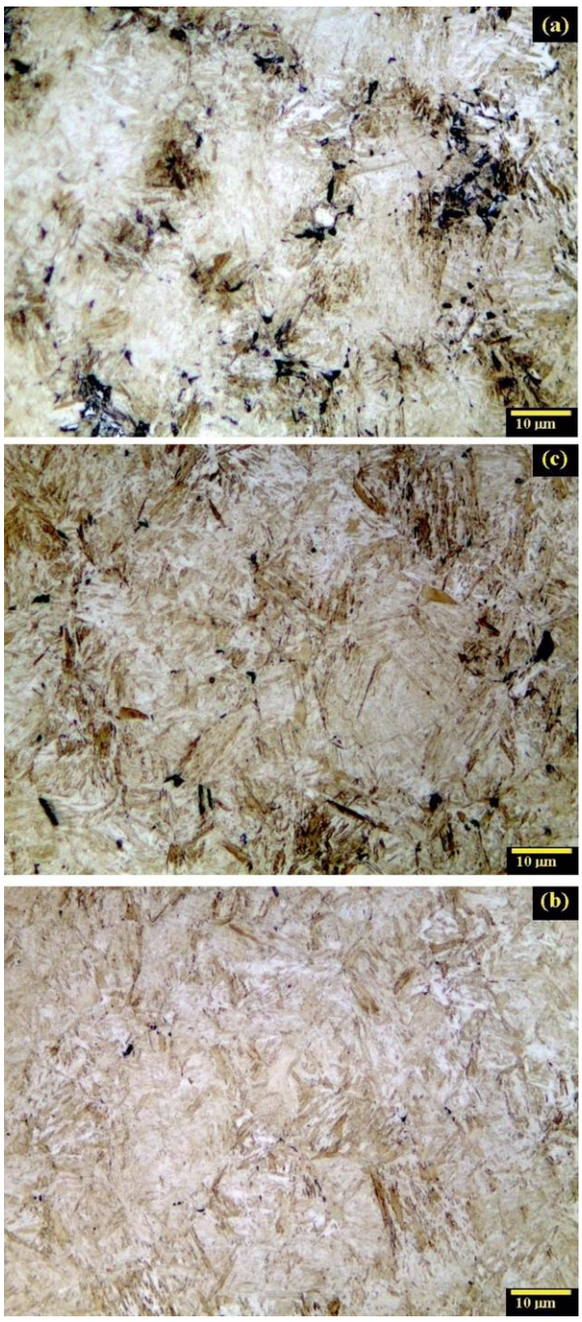

Figure 4 Optical micrographs of AISI-4045 steel samples heated by induction at a temperature of 1123 K for (a) 2.0 s, (b) 2.2 s and (c) 2.4 s and tempered in polymeric solution
Source: Own, Leco MX205M Microscope

Microhardness of the surface of hardened 1045 steel

The Vickers microhardness of the surface layer of 1045 steel subjected to induction hardening at 1123 K was found in a range of values between 709 to 744 (± 45) HV for points A, B, C and D shown in Figure 5. In general, the average microhardness values are within specification for 1045 steel treated under these conditions.

However, it is observed that at longer induction times there is an increase in hardness values, which is related to the fact that at shorter austenitic times the austenitic grain size tends to decrease due to the inverse relationship proportional to the hardness of the hardened parts. It was confirmed that short austenitizing periods generate a decrease in the hardness values for this type of steel, AISI-1045; in addition, as a function of the decrease in the austenitic grain size and the time for the dissolution of carbides during the transformation from pearlitic phase (α + Fe3C) to austenitic (γ).

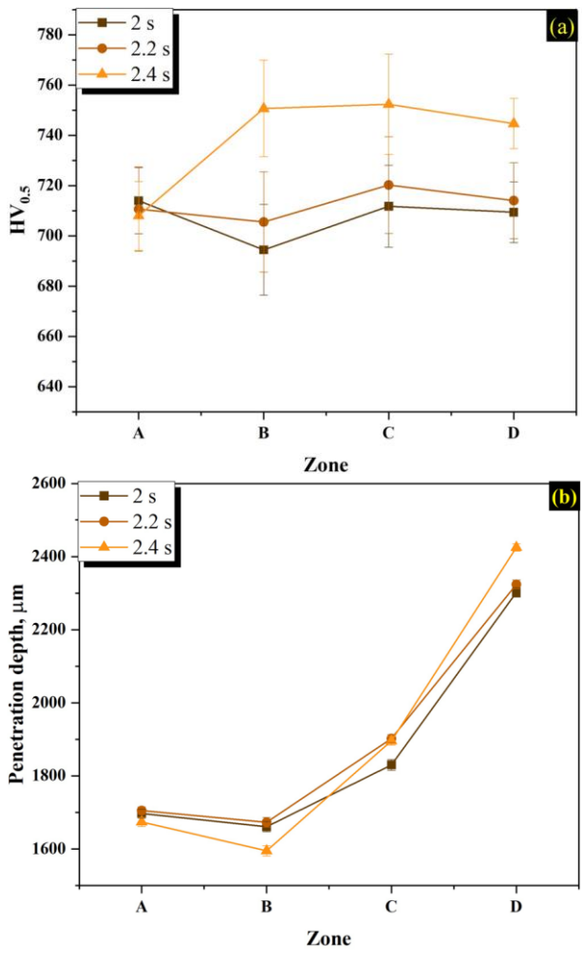

Figure 5 (a) Vickers microhardness measurements at the critical points of the automotive part indicated in Figure 1, and (b) depth of the thickness of the hardened layer in the indication quenching of AISI 1045 steel
Source: Own, Origin

HK, HV and HRC hardness equivalences

It is important to note the difficulty of converting between hardness scales, in this regard Callister [9] emphasizes that due to the fact that hardness is not a well-defined property of the material and because of the experimental differences of each technique, a general method of converting hardnesses from one scale to another.

ISSN-2531-2189

The conversion data have been determined experimentally and found to be dependent on the type of material and the characteristics. Likewise, for the conversion between scales, data have been found for steels whose data are illustrated in Figure 6. The equivalence between one scale and another is calculated roughly by drawing a horizontal line that crosses both scales and, if necessary, performs a correlation for a more exact value of the conversion between scales.

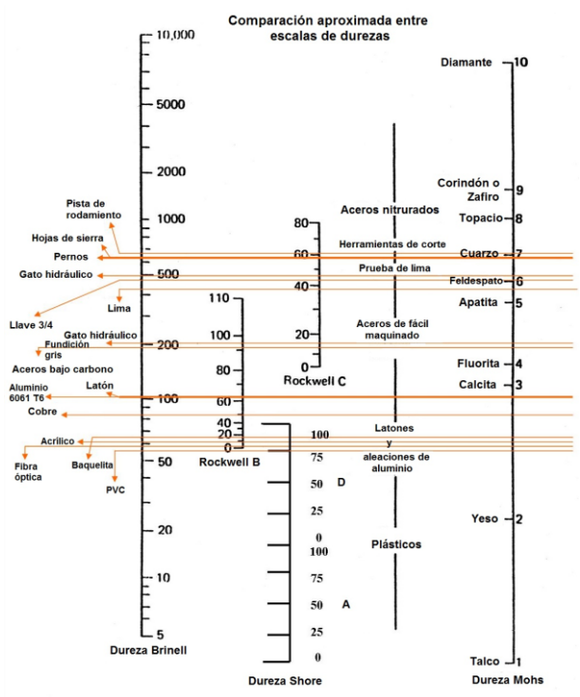

Figure 6 Schematic representation of the different hardness scales
Source: Internet

For this reason, it is necessary to establish equivalent values between the HK, HV and HRC hardness scales for AISI 1045 steel heat treated with induction heating, which is shown in Table 1. The results corroborate what was mentioned by Ghorbal *et al*. [10] where they mention that the HV / HK hardness ratio has a variation between 1.05 and 1.15. Therefore, the comparison between hardness scales should be taken with reserve; Therefore, the conversion between hardness scales is recommended only in the event that it is not possible to measure this property directly on the specified scale; Similarly, both Callister and Ghorbal *et al*. indicate that the Knoop hardness scale is more appropriate for brittle materials, so testing materials with greater ductility can generate a deviation in the hardness values determined by said scale.

Knoop hardness (HK)	Vickers hardness (HV)	Rockwell C hardness (HRC)
311	303	30
427	416	42
450	438	44
504	491	48
548	534	50
556	542	51
604	589	54
620	604	57
650	633	58
685	668	59
700	682	59
702	684	59
705	687	59
713	695	59
715	697	59
721	736	60
814	794	64
848	827	65

Table 1 Equivalences between the HK, HV and HRC hardness scales for AISI 1045 steel
Source: Own, Word

Determination of the thickness of the hardened layer

Figure 7 shows the thicknesses of the hardened layer in the four areas considered critical in the automotive part, since the surface at these points will be subjected to friction, the microhardness corresponds to large values. In the results obtained, a slight variation was observed in the measurements of the same points at the three time conditions. But, in addition, a considerable increase in the thickness of the layer was measured at points C and D. This variation was associated, not with heating by electromagnetic induction; which depends on the intensity of the magnetic field, the frequency of the working current, the separation between the piece and the inductor coil, as well as the magnetic characteristics of the material to be treated; if not to the geometric shape of the piece. In addition to the above, the austenitizing time is also a variable that influences the depth of penetration of the temper and showed a clear trend specifically at points C and D where it was observed that at austenitizing times of 2.0 and 2.2 s the thickness the layer was less; Cunningham et al. [11] indicate that the variations in the depth of the layer are due, in the case of induction by a single shot, to the exposure time of the steel above the critical temperature A3, for which it was concluded that the geometry of the piece mainly influenced the temperature reached in the different areas of the piece, and that areas A and B were exposed to a shorter time to induction heating compared to points C and D.

ISSN-2531-2189

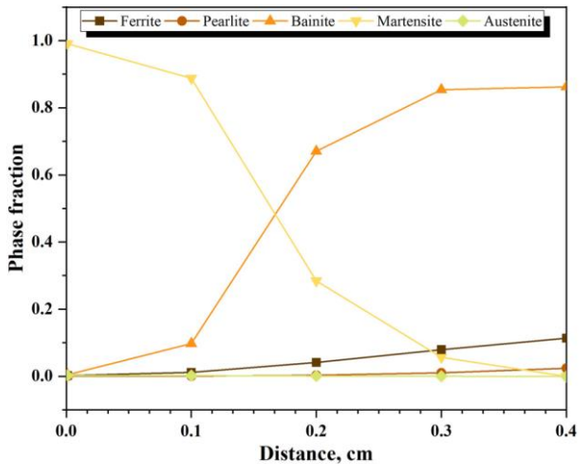

Figure 7 Phase fractions present in the Jominy test for AISI 1045 steel as a function of the penetration depth of the tempered layer
Source: Own, Origin

Figure 8 shows the results of the thermodynamic simulation with the JmatPro software, where the chemical composition of the AISI 1045 steel is considered, in addition to the ASTM grain size, whose value was determined experimentally, only for the austenitized sample for 2.4 s, and it was 9 ASTM at a temperature of 1123 K. The simulation was used in order to appreciate and confirm what was reported by Cyderman *et al*. [4], who determined that at short heating times the grain size decreases and the surface hardness of the hardened layer decreases.

The Jominy curves simulated by the thermodynamic software of Figure 8 show that with the reduction in size it generates a reduction in the hardness of the hardened layer, or in other words, the hardenability of the steel decreases with the reduction of it; this is due to the fact that a small austenitic grain size generates a greater number of precipitation centers, that is, the austenite will be less stable in austenitizing.

Stability is achieved at large grain sizes and is achieved, either by the action of temperature or time, the first condition being favorable in induction hardening, since the subjection times are short in this surface hardening technique. The results showed that in the outer layer of the material 100% of the martensitic transformation was achieved and as the distance was greater, this metastable phase gave rise to stable phases, in this case ferrite and pearlite.

Therefore, it was inferred that the hardness of the material decreased at a greater hardening depth, which was corroborated with what is shown in the simulated hardness and resistance curves of Figure 8, where it was observed that the microhardness of the material increased in the outer layer of the material, the measurement result was 684 HV at a layer depth of between 10 and 1000 µm. The above validated that the hardening capacity of the material is determined by metallurgical aspects such as the chemical composition and the austenitic grain size. It is also important to mention that the hardenability of the steel depends primarily on the carbon content, since it is fundamental for the martensitic transformation, considered as a transformation process without diffusion, in which the austenite phase distorts its face-centered cubic crystal lattice to become tetragonal.

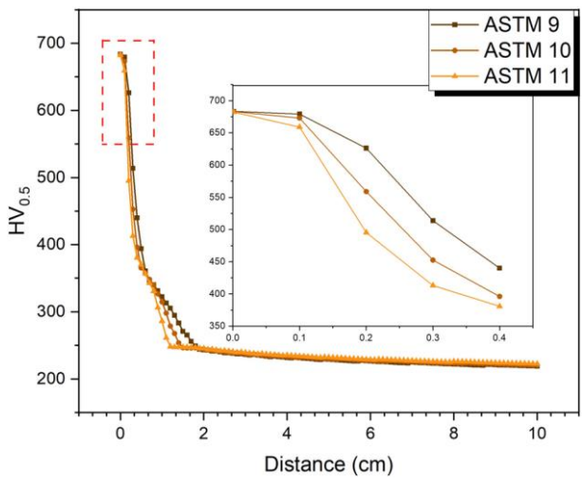

Figure 8 Simulated Jominy curves for 1045 steel as a function of austenitic grain size
Source: Own, Origin

The austenitic grain size is an important factor that determined the microstructure formed, since it influenced the phase transformation kinetics during the cooling cycle. Microstructure has been reported to have a large effect on the mechanical properties of the product, ie, it is essential to control grain size growth in heat treated alloys. Due to the above, one of the microstructural advantages of induction hardening is the refinement of the austenitic grain; the temperatures used for heating conventional Jominy specimens ensure a grain size refinement of approximately 30-40 µm (ASTM 6.5-7) [4].

ISSN-2531-2189

The samples with 2.4 s of austenitizing showed a grain size of approximately between 9-11 µm, so that in Figure 7 a slight influence on the hardenability of a finer grain size was observed. It is this same sense, Chongxiang *et al*. [12] studied the effect of the temperature and time variables on the growth of austenitic grain in GCr15 steel, finding that it grows gradually with temperature and holding time at different austenitic temperatures.

Acknowledgments

The authors thank IDEA GTO for financing through the Scientific and Technological Push program Modality 2 (AI) Support to Researchers in the SICES / CONV / 140/2020 agreement, in addition, to GH Mexicana, CIE Automotive and the UPJR for the facilities provided to the realization of this work.

Conclusions

The behavior of AISI-1045 steel subjected to a heat treatment with induction heating, was studied through the correlation of the values of microhardness (HV) and the thickness of the hardened layer at three different austenitizing times, of 2.0, 2.2 and 2.4 s at 1123 K and cooled to 301 K with a 5% polymer solution. The results of the microstructural characterization revealed that the transformation of the AISI-1045 steel, initially consisting of pearlite surrounded by allotriomorphic ferrite to martensite, occurred at the three austenitizing times tested; the final microstructure was composed of a mixture of martensite in the form of slats and plate, typical formations of steels with medium to high carbon content.

However, it was found that at a heating time of 2.0 s, the austenitizing time was not sufficient to dissolve the cementite because the grain refinement was not completed, which was verified by the presence of carbides in the microstructure of the steel treated under this condition, and that was not observed in the other times of the study. On the other hand, it was observed that at shorter austenitizing times the hardness of the layer showed a reduction in this property due to the aforementioned phenomenon of austenitic grain refinement and the incomplete dissolution of the iron carbide.

Finally, the depth of the boundary layer showed an increase in points C and D of the part that can be associated with the different exposure times to the austenitizing temperature during induction heating, mainly due to the complex geometry of the tempered part.

References

1. A. I. West C. (2010). *Standard test methods for determining hardenability of steel*. ASTM, A255-10.

2. M.A. Grossmann, et al. (1964). *Principles of heat treatment*. USA, American Society for metals.

3. Samuel J. Rosenberg. (1940). *Effect of rate of heating through the transformation range on austenitic grain size.* Journal of Research of the N.ational Bureau of Standards, 25, 215-228.

4. R. Cryderman, et al. (2020). *Effects of Rapid Induction Heating on Transformations in 0.6%*. Journal of Materials Engineering and Performance, 29, 3502–3515.

5. K. D. Clarke, et al. (2011). *Induction Hardening 5150 Steel: Effects of Initial Microstructure and Heating Rate*. Journal of Materials Engineering and Performance, 20, 161–168.

6. V. Rudnev, D. Loveless, et al. (2017). *Handbook of induction heating*. New York, CRC Press.

7. ISO 6507-1:2005. (2005). Metallic materials — Vickers hardness test — Part 1: Test method. USA, ISO/TC 164/SC 3 Hardness testing.

8. Z, J.I.S.C.J.J., Vickers hardness test-test method. 2009.

9. Callister Jr, et al. (2012). *Fundamentals of materials science and engineering: an integrated approach*. USA, John Wiley & Sons.

10. Ghorbal G.B., et al. (2017). *Comparison of conventional Knoop and Vickers hardness of ceramic materials.* Journal of the European Ceramic Society, 37, 2531-2535.

ISSN-2531-2189

11. J. Cunningham, et al. (1999). *Effects of induction hardening and prior cold work on a microalloyed medium carbon steel*. Journal of Materials Engineering and Performance, 8, 401-408.

12. C. Yue, et al. (2010). *Kinetic Analysis of the Austenite Grain Growth in GCr15 Steel*. Journal of Materials Engineering and Performance, 19, 112-115.

ISSN-2531-2189

Article **Journal of Mechanical Engineering**
June 2021 Vol.5 No.15 16-23

The numerical characterization of the gas turbine blade with static stress analysis applying finite element method

La caracterización numérica del álabe de la turbina de gas con el análisis de esfuerzos aplicando el método de los elementos finitos

VILLAGRÁN-VILLEGAS, Luz Yazmín†*´,´´, HERNÁNDEZ-GÓMEZ, Luis Héctor´, MARTÍNEZ-CRUZ, Miguel Ángel´ and ROJAS-RAMÍREZ, Jorge Armando´

´Instituto Politécnico Nacional, School of Mechanical and Electrical Engineering, Graduate Studies and Research Section, Unidad Profesional Adolfo López Mateos "Zacatenco", Building 5 Floor, Lindavista, Zip. 07738, Mexico City.
´´Universidad de Veracruz, Faculty of Electrical Mechanical Engineering, Venustiano Carranza St. no number, Revolution, Ave. Zip. 93390, Poza Rica; Veracruz, Mexico.

ID 1st Author: *Luz Yazmín, Villagrán-Villegas* / **ORC ID:** 0000-0003-3860-2923, **CVU CONACYT ID:** 96365

ID 1st Co-author: *Luis Héctor, Hernández-Gómez* / **ORC ID:** 0000-0003-2573-9672, **CVU CONACYT ID:** 5107

ID 2nd Co-author: *Miguel Ángel, Martínez-Cruz* / **ORC ID:** 0000-0002-4431-9262, **CVU CONACYT ID:** 208501

ID 3rd Co-author: *Jorge Armando, Rojas-Ramírez* / **ORC ID:** 0000-0002-0779-1242, **CVU CONACYT ID:** 120643

DOI: 10.35429/JME.2021.15.5.16.23 Received January 20, 2021; Accepted June 30, 2021

Abstract

The lifespan of a blade is reduced due to the operating environment and high mechanical and thermal stresses, where typically two or more factors act simultaneously. The most common degradation mechanisms are: contamination, blade pitting, opening of the gap between rotor and stator, and erosion of the leading and trailing edge of the gas turbine blade. Degradation is mainly caused by scale, corrosion, hot corrosion, oxidation, erosion, abrasion, particle melting and mechanical degradation. The research that has been carried out in turbine blades are based on visual observations, optical microscopy, scanning electron microscopy, fractography analysis, metallography, structural analysis and hardness tests. This work proposes a methodology to carry out numerical analysis of the nozzle blade of a gas turbine. The investigation will perform a scan to obtain a 3D model using reverse engineering. Reverse engineering technology can be used to assist in the manufacture of replacement parts when the original parts inventory is depleted. The numerical analysis with the point mesh of the nozzle blade and static stress modeling in ANSYS were made. The main objective of this work is to know the maximum and minimum values at which a turbine blade is operating and located the area of the gas turbine blade is more prone to failure due to different wear mechanisms and to the stresses that the blades are subjected during the operation of the gas turbine.

Blades, Gas turbine, ANSYS, Static modeling

Resumen

La vida útil de un álabe se reduce debido al entorno de funcionamiento y a las elevadas tensiones mecánicas y térmicas, donde suelen actuar dos o más factores simultáneamente. Los mecanismos de degradación más comunes son: la contaminación, las picaduras en los álabes, la apertura del claro entre el rotor y el estator, y la erosión del borde de ataque y de salida del álabe de turbina de la turbina de gas. La degradación se debe principalmente a las sales, la corrosión, la corrosión en caliente, la oxidación, la erosión, la abrasión, la fusión de partículas y la degradación mecánica. Las investigaciones que se han llevado a cabo en los álabes de turbina se basan en observaciones visuales, microscopía óptica, microscopía electrónica de barrido, análisis de fractografía, metalografía, análisis estructural y ensayos de dureza. Este trabajo propone una metodología para realizar el análisis numérico del álabe de la tobera de una turbina de gas. La investigación realizará un escaneo para obtener un modelo 3D mediante ingeniería inversa. La tecnología de ingeniería inversa puede utilizarse para ayudar a la fabricación de piezas de repuesto cuando se agota el inventario de piezas originales. Se realizó el análisis numérico con la malla de puntos del álabe de la tobera y el modelado de la tensión estática en ANSYS. El objetivo principal de este trabajo es conocer los valores máximos y mínimos a los que opera un álabe de turbina y localizar la zona del álabe de turbina de gas más propensa a fallar debido a los diferentes mecanismos de desgaste y a las tensiones a las que están sometidos los álabes durante el funcionamiento de la turbina de gas.

Álabes, Turbina de gas, ANSYS, Modelado estático

Citation: VILLAGRÁN-VILLEGAS, Luz Yazmín, HERNÁNDEZ-GÓMEZ, Luis Héctor, MARTÍNEZ-CRUZ, Miguel Ángel and ROJAS-RAMÍREZ, Jorge Armando. The numerical characterization of the gas turbine blade with static stress analysis applying finite element method. Journal of Mechanical Engineering. 2021. 5-15:16-23.

* Correspondence to the Author (Email: yvillagran@uv.mx)
† Researcher contributing as first author.

Introduction

Gas turbines play an important role in fields such as aviation and power generation. The main function of blades in gas turbines is to use or extract energy from a fluid stream to change the speed and pressure of the fluid flow. In the absence of design data, the reverse engineering process can be considered an important tool for modeling. The reverse engineering process involves detecting the geometry of the blade, creating a geometric model from the detected data, and passing this model to an appropriate CAD / CAM system for fabrication. (Gopinat, 2014)

Turbine blades are subject to complex conditions of temperature, stress, oxidation and hot corrosion (Giampaolo, 2016). The extreme service environment often results in premature failure of the turbine blades, when the turbine inlet gas temperature exceeds the service temperature limit, the turbine blades are subjected to overheating; this could lead to rapid microstructural degradation and even brittle fracture. (Xiaotong, 2016) Gas turbine efficiency in oil & gas applications has improved more than 40%, currently, leading OEM manufacturers and researchers are working on gas turbine optimization design to constantly improve efficiency and reduce cost of gas turbines maintenance (Jun Su, 2019).

To further increase the thermodynamic efficiency of advanced gas turbines, higher gas inlet temperatures are required. An increase in the gas inlet temperature causes an increase in thermal stresses throughout the engine, especially in the turbine blades and therefore drastically reduces its useful life. Experimental research of turbine blade materials under real operating conditions are very demanding Figure 1 shows seventh stage compressor blade; thermal and mechanical analysis must be performed based on the finite element method (O Kaussa, 2019).

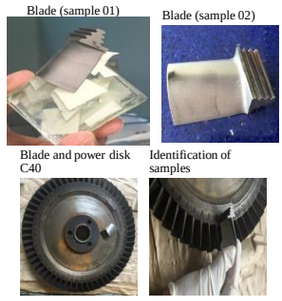

Figure 1 Rotor blades of axial compressor.
Note. Adapted from Turbine Compressor Disc, Villagrán-Villegas Luz Yazmin, 2017

Turbine blades are subject to stresses because of high temperatures, high centrifugal forces, and thermal cycling; these stresses accelerate the growth of defects that may be present in the material; this is the base of the demand for materials that can withstand high temperatures without losing their resistance to centrifugal forces, vibrations, thermal cycles, oxidation or corrosion.

The improvement in creep and rupture strength properties was constant from the late 1940s to the early 1970s, since 1960, the reliance on sophisticated cooling techniques for turbine blades and nozzles has increased. The increase in the turbine inlet temperature was possible thanks to new air-cooling schemes and the incorporation of complex ceramic core bodies used in the production of hollow and cast parts, Figure 2 shows two elaborated compressor blades of a chromium superalloy and a power turbine blade with red coloration due to the exposure of the ceramic coating to high temperatures in the first power stage.

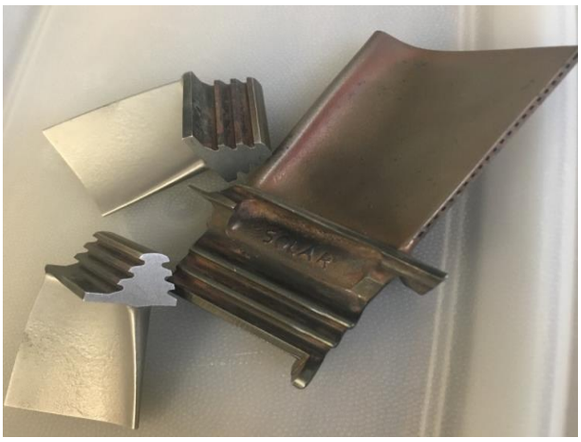

Figure 2 Two rotor blades of an axial compressor and a power turbine blade
Note. Adapted from Turbine Compressor Disc, Villagrán-Villegas Luz Yazmin, 2017

ISSN-2531-2189

VILLAGRÁN-VILLEGAS, Luz Yazmín, HERNÁNDEZ-GÓMEZ, Luis Héctor, MARTÍNEZ-CRUZ, Miguel Ángel and ROJAS-RAMÍREZ, Jorge Armando. The numerical characterization of the gas turbine blade with static stress analysis applying finite element method. Journal of Mechanical Engineering. 2021

Protective coatings used on turbine blades were developed to serve as physical barriers between the aggressive environment and the substrate. (Jaroslav,2010)

In addition, Thermal Barrier Coatings are used as a cover material, delay creep degradation and reduce the severity of thermal gradients; no coating has been found that can fully survive the aggressive turbine environment. The durability of thermal barrier coatings is limited by degradation of adhesion by environmental interactions rather than mechanical stress. (Miller, 2010)

The most serious degradation modes are as follows: oxidation of high temperature, hot corrosion, damage due to thermal and thermomechanical fatigue, mechanical damage from erosion and creep degradation during overheating.

Solar Turbines' Centauro 40 gas turbine operates in the active Bellota-Jujo complex located in the city of Comalcalco, 30 km from Villahermosa, Tabasco, the fields are in the municipalities of Comalcalco, Paraíso, Jalpa de Méndez, Nacajuca, Cunduacán, Cárdenas and Huimanguillo.

The area represents the greatest oil wealth in southeastern Mexico, due to the quality of its hydrocarbon and because of the giant fields that have been discovered there. (Córdova, 2011) The Centauro 40 turbine has the following normal operating conditions, shown in Figure 3: Inlet temperature, inlet air pressure, sensing of 5 temperatures of the third power turbine stage (T5), alarms and compressor efficiency (NGP) and in power turbine (NPT). (Padilla, 2021)

Figure 3 C40 Gas Turbine Operation Summary
Note. Adapted from Blade Wear Analysis of TG C40, Villagran-Villegas Luz Yazmin, 2017

Fabrication materials for centaur 40 gas power turbine blades

The following figure shows a graph that contains the elements that make up the Centaur 40 gas turbine blade as well as their percentage that each element occupies, made from a chemical analysis, in a scanning electron microscope.

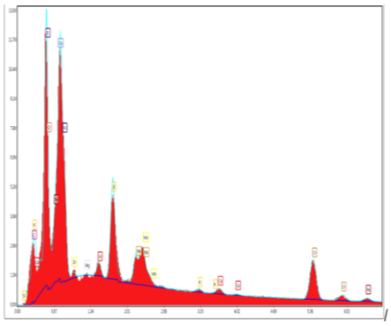

Elemento	Peso %
C K	10.04
O K	13.12
Fe L	5.15
Co L	24.12
Ni L	8.83
Zn L	0.59
Mg K	0.05
Al K	0.68
Si K	5.11
Nb L	3.95
Mo L	3.72
K K	0.41
Ca K	0.94
Cr	23.2

Figure 4 Chemical elements of the C40 gas turbine compressor blade
Note. Adapted from TG Blade Wear Analysis, Villagran-Villegas Luz Yazmin, 2017, ***b***

Methodology

The methodology of the numerical analysis will be developed in five stages (Figure 5), which are the following:

1) First stage: Know the operating conditions of the gas turbine.

2) Second stage: Obtaining the samples to be analyzed (power turbine blades).

3) Third stage: Acquire the model in a point cloud from the original model. (reverse engineering).

4) Fourth stage: Numerical analysis and simulation in static state supported by engineering software (ANSYS).

5) Fifth stage: Research conclusions.

ISSN-2531-2189

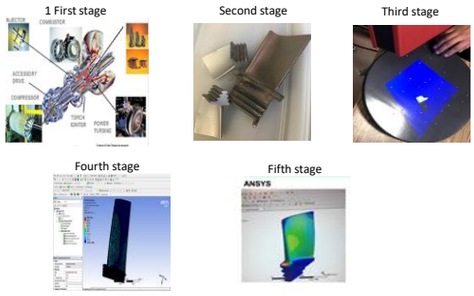

Figure 5 Methodology of numerical analysis.
Note. Adapted from Study on the damage caused by wear in the blades of a gas turbine compressor *(Villagrán-Villegas Luz Yazmin, 2017)*

A. Determination of operating conditions.

Figure 6 Blade sample after its operation in the Northeast Region, in the Cantarell asset, Nohoch Alfa Oil Platform

The sample in Figure 6 was in operation in the Northeast Region, in the Cantarell asset, Nohoch Alfa Oil Platform. The air enters the gas turbine at room temperature of 15 ° C (at the sea level) and increases its temperature when compressed, reaching 1,800 ° C, after passing through the combustion chambers. The Centaur 40 turbine is made up of 11 stages. In the axial type of compressor, the pressure ratio is 10.3: 1 and the air flow input is 18.7 kg / sec (41.3 lb / sec). The variable vanes begin to open when the Pcd (pressure compressor discharge) reaches approximately 32 psi (gauge) and fully open when the Pcd reaches approximately 76.5 psi (gauge).

Table 1 shows the information provided by the manufacturer and Table 2 the sample data.

Condition	Value
Compressor discharge pressure (PCD)	107.5 psi (lb/in^2)
Average temperature of thermocouple T5	1400 ºF
Gas Producer Speed **NGP.**	95.9 %
Power Turbine Speed) **NPT.**	84.8 %

Table 1 Turbine C40 data

Sample	Material	Stage	Weight
Blade	Superalloy	1	42.37 g

Table 2 Power turbine blade data

B. Obtaining samples.

The ATOS ScanBox (Figure 7) is a 3D optical measurement equipment that was developed by GOM for efficient quality control in the production and manufacturing process; it is an optical 3D coordinate measuring system.

Figure 7 ATOS ScanBox

ATOS sensors provide full-field 3D coordinates for each individual measurement of up to 16 million independent measurement points and are captured within 1 to 2 seconds. The measurement data is characterized by a very detailed reproduction and therefore also allows the measurement of very small components (38mm).

ATOS captures the entire surface geometry of an object accurately in a dense point cloud or polygon mesh; that enable detailed, high-resolution scans, rapid data collection, advanced inspection functionality, and comprehensive dimensional analysis. GOM Inspect is software for 3D measurement data analysis. GOM software is used in product development, quality control, and production. The generated model is a polygonal mesh that can be smoothed, thinned and refined, likewise, from the initial model, the holes in the mesh can be filled, allowing curvatures to be extracted. The mesh is processed using algorithms based on curvatures and tolerances. The software provides the user with a view prior to each processing step and generates the calculation of an average mesh.

ISSN-2531-2189

Once the scanner assembly and calibration process has been carried out, it is time for the digitization of the part that we want to evaluate in this particular case it is the blade of a gas turbine.

The scanner works in an optimal way when the piece is white, since there is a difference in tones, in addition to eliminating the reflection in the metallic pieces, which makes the sensor perfectly detect the details, thus achieving a model. STL similar to the original part.

If the piece to be scanned is not white, there is a procedure, which consists of applying a zinc oxide coating that manages to change the original color and at the same time eliminates the excess shine that a metallic piece can get. to be reflected, thus guaranteeing optimal performance by the scanner.

Our sample to be scanned (blade) will require the application of a zinc oxide coating due to its color tone (Figure 8).

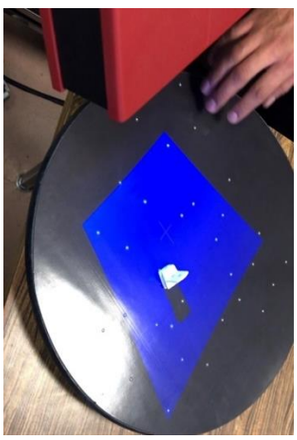

Figure 8 Zinc oxide coated blade.
Note. Adapted from Study on the damage caused by wear in the blades of a gas turbine compressor, Villagrán-Villegas Luz Yazmin, 2017.

C. 3D model

The piece to be scanned must be completely dry after applying the zinc oxide coating, to start the digitization process; For this, sample holder clips and stickers are used that will serve as reference points when closing our piece after scanning. (Figure 9)

Figure 9 Blade with reference points
Note. Adapted from Study on the damage caused by wear in the blades of a gas turbine compressor, Villagrán-Villegas Luz Yazmin, 2017.

The piece is placed on a rotating base full of reference points that will help us to obtain digitization. Once the light bombardment process has started by the scanner, the part cannot be moved from its original position. As soon as the software detects that the part and all the reference points are in the correct position, the equipment will begin to scan and obtain the first parts of the point cloud (Figure 10) represented with the parts in red.

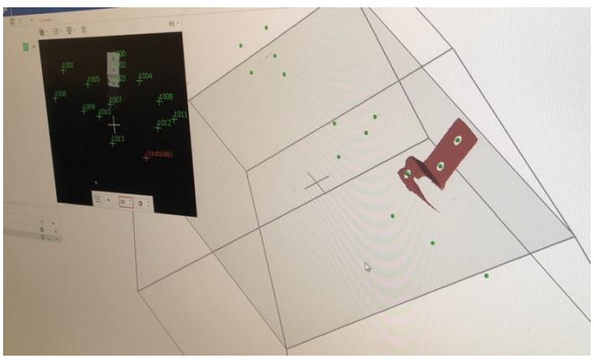

Figure 10 Power turbine blade point cloud

At the end of the necessary scans, the two measurement series will be joined using the reference points to obtain a single point cloud that combines the two measurement series, which shows us a form very similar to the real one. The process of scanning a part is a very exact process. Reverse engineering is used since a design is obtained from a product. Without a doubt, the point cloud obtained through the ATOS & GOM scanner closely matches the actual design of the piece. Once the entire process has been carried out, the .STL file is obtained, which offers us endless possibilities, either by solidifying the model to be able to simulate it in some engineering software or by transforming it to another format readable by a 3D printer to finally print it.

ISSN-2531-2189

D. Numerical analysis.

To overcome the difficulty of solving real continuous problems, engineers and mathematicians have been proposing, over the years, various methods of discretization. The application of these methods makes it necessary to carry out some approximation, in such a way that it can be expected that it approaches, as closely as desired, the true continuous solution as the number of discrete variables increases. (Cuevas,2017)

The unique way of approaching discrete type problems leads us to the definition of the finite element method as an approximation procedure for continuous problems, in such a way that:

a) The continuum is divided into a finite number of parts (elements), whose behavior is specified by a finite number of parameters.

b) The solution of the complete system as an assembly of the elements follows precisely the same rules that apply to discrete type problems.

The Finite Element Method uses the discretization hypothesis, which is based on the following:

- The continuum is divided by means of imaginary lines or surfaces into a series of contiguous and disjoint regions of simple and normalized geometric shapes, called finite elements.

- Finite elements are joined together at a finite number of points, called nodes.

- The displacements of the nodes are the basic unknowns of the blade structure and this determine the deformed configuration of the structure.

- The displacement of any point is uniquely determined by the displacement of nodes of the element to which the point belongs and interpolation functions are defined for each element that allow the calculation of the value of any interior displacement by interpolating the nodal displacements.

- The interpolation function and the nodal displacement defined the state of strains inside element.

- For each element, there is a system of forces concentrated in the nodes, which balance the tension in the element contour and the external forces acting on it.

- The solution function of the problem is approximated independently in each element. The solution function is approximate within each element, relying on a finite (and small) number of parameters, which are the values of said function in the nodes that make up the element and sometimes its derivatives. (Celigüeta, 2019)

Due to the characteristics of the scanned blade geometry, our .STL file has a total of 688,076 facets (Figure 11). If you zoom in on any region, you can see a large number of facets into which our point cloud is divided.

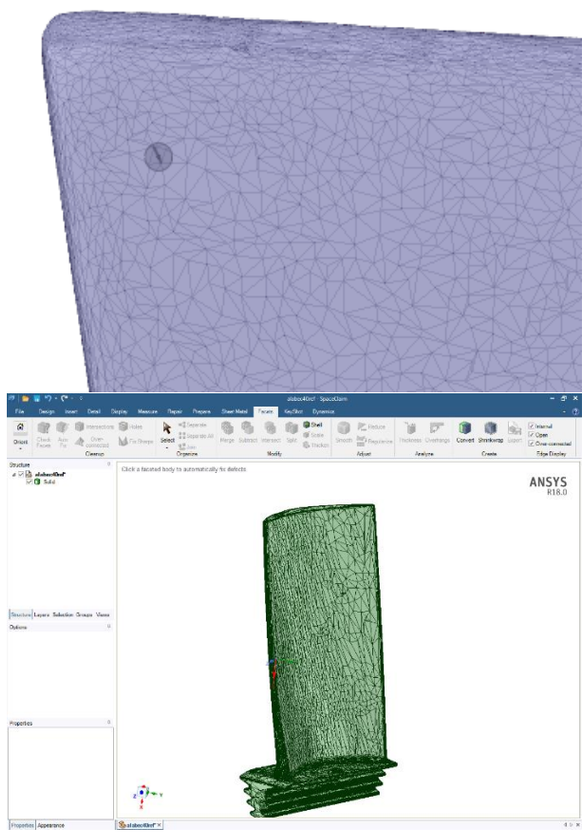

Figure 11 Power turbine blade mesh with 688,076 facets

Results

The values of the variables used in the stationary stress analysis (type: Von Mises) in the blade are: (Figure 12).

Material: Base Superalloy Cr (Losertová, 2014)

Module of Young 0.211 Gpa (Losertová, 2014)

Density: 8.35 x 10 3 kg/m3 (Losertová, 2014)

Relation of Poisson: 0.325 (Losertová, 2014)

Fluid stress: 0°-15 ° (Solar, 2007)

Air pressure: 110 psi (Solar, 2007)

Maximum stress: 158.31 Mpa (Solar, 2007)

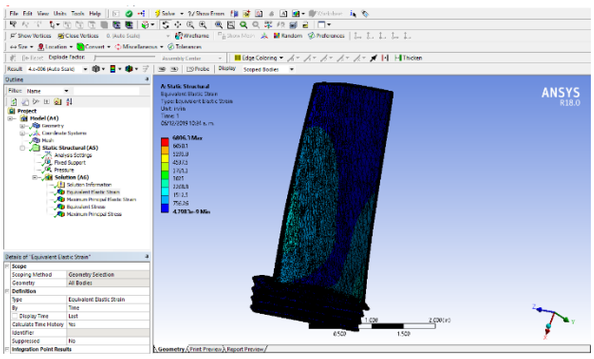

Figure 12 1st stage power turbine blade

Conclusions

The simulation of a gas turbine blade from the power turbine area was achieved.

In the project, 3D models of the blade were obtained, through the ATOS & GOM optical scanner (tool provided by the National Polytechnic Institute), of which a dotted mesh with 688,076 facets was recorded.

With the SpaceClaim software, the solidification of the model obtained was obtained.

Finally, a static analysis was carried out with the help of the ANSYS Workbench R18.0 software, where the characteristics of which the blade material is made were added, as well as the application of a mesh (Figure 13).

The work concluded with a Finite Element Analysis, with a pressure of 107.5 psi distributed in the intrados of the blade, obtaining a maximum Von Mises effort of 1.873e5 (psi) and a minimum of 1.321e-7 (psi) with a total of 367,381 nodes and 217,272 elements.

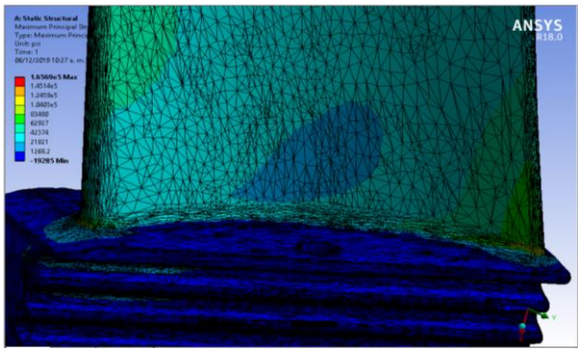

Figure 13 Finite element analysis in the power turbine blade

Acknowledgements

The authors of this research gratefully acknowledge the Instituto Politécnico Nacional (IPN), Mexico, for their support for the development of this work.

References

Hutchings, I. (2003). Tribology (Vol. 1). (B. Heinemann, Ed.) London, UK: Elsevier Science.

Villagrán-Villegas, L.Y. (2017). Estudio sobre el daño causado por desgaste en los álabes de compresor de una turbina de gas, 4, 94.

Gopinath Chintala, P. G. (2014). Optimum material evaluation for gas turbine blade using.

Giampaolo, A. (2006). Gas Turbine Handbook; Principles and practices (3a. ed., Vol. 1). (CRC, Ed.) BR, Florida, USA: The fairmont press.

Xiaotong Guoa, W. Z. (2019). Evaluation of microstructural degradation in a failed gas turbine blade due to overheating. ELSEVIER, Engineering Failure Analysis.

Jun Su Parka, W. C. (2019). Heat and mass transfer characteristics on the first-stage gas turbine blade under unsteady wake flow. ELSEVIER, International Journal of Thermal Sciences.

O Kaussa, H. T. (2019). Structural analysis of gas turbine blades made of Mo-Si-B under transient T thermo-mechanical loads. ELSEVIER, Computational Materials Science.

Jaroslav Pokluda, M. K. (September de 2010). Damage and Performance Assessment of Protective Coatings on Turbine Blades. Intech.

ISSN-2531-2189

Miller, R. A. (March de 2009). History of Thermal Barrier Coatings for Gas Turbine Engines. NASA STI Program .

Cordova Lopez Fernando, L. F. (2011). Administracion de proyectos de explotación. Universidad Veracruzana, Coatzacoalcos.

Padilla, N. N. D., & Silvera, A. J. B. (2021). Diseño de sistemas termofluidos: una visión integradora. Ediciones de la U.

Cuevas, E. (2017). Tratamiento de Imágenes con Matlab.

Celigüeta, L. (2019) Método de los Elementos Finitos para Análisis Estructural. Unicopia CB

Losertová, M. (2014). Advancved materials (Vol. 1). (VSB, Ed.) Ostrava: VSB.

Solar Turbines A Caterpillar Company. (2007). Curso de operación y mantenimiento rutinario (Vol. 1). San Diego, C.A., USA: Solar Turbines Incorporated.

ISSN-2531-2189

Article **Journal of Mechanical Engineering**
June 2021 Vol.5 No.15 24-31

Vibration analysis in a rotodynamic system

Análisis de vibraciones en un sistema rotodinámico

GAMBOA-MARTÍN, Vianney Aurora†*, RODRIGUEZ-BLANCO, Marco Antonio, DURÁN-MORALES, Iván and MARTÍNEZ-RODRÍGUEZ, Gilberto

Universidad Autónoma del Carmen, Faculty of Engineering and Technology, México.

ID 1er Author: *Vianney Aurora, Gamboa-Martín* / **ORC ID**:0000-0001-6257-5473, **Researcher ID Thomson**: AAN-2297-2021, **CVU CONACYT ID:** 1015116

ID 1er Co-author: *Marco Antonio, Rodríguez-Blanco* / **ORC ID**:0000-0003-3641-6895, **Researcher ID Thomson**: U-6476-2017, **CVU CONACYT ID:** 92331

ID 2do Co-author: *Iván, Durán-Morales* / **ORC ID**: 0000-0001-9568-4457, **Researcher ID Thomson**: AAQ-1775-2021, **CVU CONACYT ID:** 169683

ID 3er Co-author: *Gilberto, Martínez-Rodríguez* / **ORC ID**:0000-0002-3529-7460, **Researcher ID Thomson:** AAN-3256-2021, **CVU CONACYT ID:** 1015109

DOI: 10.35429/JME.2021.15.5.24.31 Received January 25, 2021; Accepted June 30, 2021

Abstract

In this paper, a study of vibrations for a rotodynamic system connected to a three-phase induction motor with mass imbalance is analyzed. The study is carried out using a test bench interacting with different scenarios of mechanical speed and rotational mass imbalance and translational mass imbalance. The critical rotational mass imbalance causes maximum vibration, then vibration and current signals are measurement in the rotodynamic and motor system respectively, which are processed and analyzed in the frequency domain. The operation scenarios of the rotodynamic system focus on the parametric variation as, separation of bearing, inertial mass unbalance and speed of the induction motor. The instrumentation for data acquisition is made up of accelerometers, current meters, frequency inverter. Open programming in LabVIEW is used to process the signals. Finally, the measured vibration, the faults found, the problems of the faults and the operation of the process are explained.

Rotodynamic system, Out-of-phase, Unbalance

Resumen

En este trabajo se analizan las vibraciones en un sistema rotodinámico conectado a un motor de inducción trifásico, las cuales son causadas por desequilibrio o desbalance de masa. El análisis se lleva a cabo interactuando con distintos escenarios y se induce a una rotación al sistema por medio de un banco de pruebas, donde un desbalance de masa en el disco lleva aun estado de excitación máxima, forzándolo a vibrar de manera desequilibrada, este entrará en un estado desequilibrado, se adquieren las señales de vibración y la corriente del motor. Las cuáles se procesan y analizan en el dominio de frecuencia. Los escenarios de operación del sistema rotodinámico se enfocan a la variación paramétrica de: separación de chumacera, masa de desbalance disco inercial y velocidad del motor de inducción. La instrumentación para la adquisición de datos está constituida por acelerómetros, medidores de corriente, variador de frecuencia. Para procesar las señales se utiliza una programación abierta en LabVIEW. Finalmente, se explica la vibración desequilibrada, fallas que esta misma ocasiona, se expone la importancia de la problemática de este, se detalla el proceso y equipo utilizado para su realización.

Sistema rotodinámico, Desfasamiento, Desbalance

Citation: GAMBOA-MARTÍN, Vianney Aurora, RODRIGUEZ-BLANCO, Marco Antonio, DURÁN-MORALES, Iván and MARTÍNEZ-RODRÍGUEZ, Gilberto. Vibration analysis in a rotodynamic system. Journal of Mechanical Engineering. 2021. 5-15:24-31.

* Correspondence to the Author (Email: paraiso_610@hotmail.com)
† Researcher contributing as first author.

Introduction

Most rotational machines contain drive systems with motors, clutches, gears, shafts, belts or chains, ball bearings, rollers, oil. Some normal vibrations can be generated by inherent machine oscillations as shaft oscillations, angular velocity, or pulse excitation in the driver. However, changes in these vibrations and additional appearances can be caused by failures. Therefore, vibration analysis is a well-established field in the supervision and monitoring of machines. In this sense, there is a machine transfer behavior between the source of the vibrations and the location of the measurement. This transfer behavior, usually expressed by a frequency response, $Gm(i\omega)$ may contain one or more resonance frequencies $\omega_{res,i}$ de the structure of the machine, as result of different mechanical systems type mass-spring-damper. There are measuring instruments in the machines such as lateral accelerometers in one, two or three directions, this direction can be orthogonal, horizontal, vertical, and axial or rotational in the casing of the machines. The measurement principle of accelerometers is based on the measurement of forces, such as the measurement of force in piezoelectric sensors, or measurement of displacement in a seismic mass using inductive sensors. Usually a high-pass filter is placed after the accelerometer to dampen low-frequency disturbances, with a cut-off frequency 100-200 Hz. Instead of acceleration $a(t)$ you can also measure the vibration speed $v(t)$or vibration displacement $d(t)$. (Isermann, R., 2005).

Machine failures generate additional stationary harmonic signals or pulse signals (Isermann, R., 2005). The former arises due to linearly overlapping effects such as imbalance, inaccurate alignment of electrical flow in electric motors, or changes in the periodic operation of the machine. The resulting signals may appear as additive vibrations, such as

$$y(t) = y_1(t) + y_2(t) + \cdots + y_n(t) = \sum_{i=1}^{n} y_i(t) \quad (1)$$

The Fourier transform is a tool that allows decomposing a function into an infinite series of functions that have different frequencies, and all of them are multiples of the frequency. (Marin, 2012).

The components of a system (bearings, pillow blocks, bearings, etc.) with the overtime suffer some wear or misalignment derived from misalignment or mass imbalance or other cause, causing the system to vibrate in an over-excited manner, then the vibration analysis is important because the failures derived from unbalanced vibration are detected, so a constant vibration wears out the components of the system.

In general, exist two types of maintenance, predictive and corrective. The predictive maintenance identifies the prevailing amplitudes in the vibration signals taken from the system, which are analyzed to determine the causes of the vibration. In this way, a scheduled stop can be established to perform preventive maintenance and correct the imbalance or replace the damaged element, subsystem or system in a timely manner and avoid the propagation of the failure. Corrective maintenance is used based on intervention or interruption in case of failure due to breakdown, which is distinguished by two ways (Blanco-Ortega, 2010) that consist of corrective maintenance by intervention with the elimination of the failure due to breakdown, where in emergency repair, replaces the damaged components of the machine, and corrective maintenance by interruption with elimination of causes, where the damaged components are replaced and the cause that originates the failure is eliminated.

The corrective maintenance it has its advantages and disadvantages, which can maximize the use of the machine or even lower the level of useful life of the same.

Various phenomena can impair the performance of induction motors and cause potential safety risks, this can be detrimental to the critical applications. Deficiencies such as unbalanced voltages due to variations in the electrical, mechanical unbalance system or harmonic grid at the voltage source could lead to problems such as excessive losses, overcurrents, mechanical oscillations, and interference in the electronic control.(Ioannides, M. G., 1995).

Starting a three-phase induction motor with unbalance in both the mechanical and electrical parts, causes vibrations in the system and increases the heating in the mechanical transmission, which propagates to the motor.

ISSN-2531-2189

The traditional method for analyzing motor operating conditions with unbalanced supply voltages has been the theory of symmetrical components. (W. H. Kersting, March/April 1997).

Common sources that generate mechanical vibrations in rotating machinery are mainly imbalance, resonances, and misalignment. The imbalance occurs when the main axis of inertia does not coincide with the geometric axis of the system, causing vibrations that generate forces that are transmitted mainly to the supports or bearings.

Vibration caused by imbalance is a common problem that occurs in a large number of rotating machineries. To balance the system, various passive and active methods or devices have been proposed with the aim of attenuating the vibrations caused by the imbalance, (Blanco-Ortega, 2010)prior to a vibration analysis.

Fault detection and diagnosis while the system is in operation helps reduce all types of losses. The mechanical failures, the uses, the slack cause different noises and vibrations with different amplitude and frequency compared to the sound and normal movement of the equipment. In this sense, the induction motors are present in all processes and systems and for this it is important to know the types of failures that can occur during their operation(Ágoston, 2015).

The voltage source imbalance and harmonic voltage distortion affect electrical power, torque, and vibrations in induction motors, for example in (Donolo, 2016) the frequency of electrical power, torque, and vibration oscillations due to voltage imbalance and harmonics is calculated. It is also shown that the typical values of harmonic distortion combined with the maximum levels of voltage imbalance allowed by the standards are sufficient to introduce vibration levels under which continuous operation of the three-phase induction motor is not recommended. Nevertheless, also the mechanical vibrations can be used to identify defects arising from defective design, faulty installation, and wear and the frequency of the measured vibration is the same as that of the force causing the vibration (Gopinath, 2010, September).

Measurement and instrumentation

The rotodynamic system or process used in this work is a mechatronic system, which consists of a three-phase induction motor connected and controlled by a frequency inverter (PowerFlex 525), in addition to and shaft or mechanical axis.

Figure 1 shows the rotodynamic system and the frequency inverter used to control the motor speed, it should be noted that the connection of the induction motor is configured in delta with the intention of ensuring the appropriate measurement between phases and dispensing with the neutral wire. In addition, the harmonic 3ra, in a delta configuration, is not magnified by the motor failure due to loss of insulation or ground fault inherent in the failures in the mechanical system.

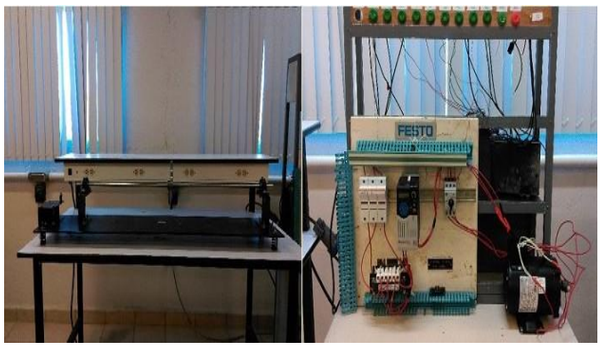

Figure 1 Rotodynamic system and PowerFlex 525 driver
Source: UNACAR mechatronics laboratory facilities

Table 1 shows the operating parameters of the three-phase induction motor with which it operates, the data in the frequency driver (PowerFlex 525) is configured through the ethernet type connection.

Motor parameters	
Volts	220 V
RPM	1725 RPM
Poles	4
Frequency	60 Hz
Current	0.9 A
HP	0.37 kW

Table 1 Three-phase induction motor parameters
Source: Own elaboration

The data acquisition (DAQ), is shown in figure 2 and consists of the following equipment:

- Sound and vibration input module NI-9234, 4 cannel, 51.2 KS/s channel ±5V.

ISSN-2531-2189

- Device USB 6003 de I/O Multifuntion, 8 I (16Bits, 100 KS/s, 2AO (5 KS/s channel), 13 DIO)

- Counter of 32 Bits, el chassis cDA-914

- Two accelerometer PCB of general purpose, 10 mV/g, ICP (EPE) GPTC03

Figure 2 DAQ equipment, target NI 9234, National Instruments
Source: Own elaboration

Methodology

The data collection methodology begins, as shown in figure 3, by programming the initial scenario with the help of the PowerFlex frequency inverter control software through an ethernet connection, subsequently the frequency variation interacts with the induction motor variation and transfers the rotational movement to the rotor, which is connected to the mechanical shaft of the rotodynamic system, an accelerometer or vibration sensor for each bearing, is connected to DAQ which is connected to the PC, where the processing and analysis using LabVIEW software with open source algorithms is developed in this work. Once the test is obtained, subsequent scenarios are carried out to obtain a more complete analysis.

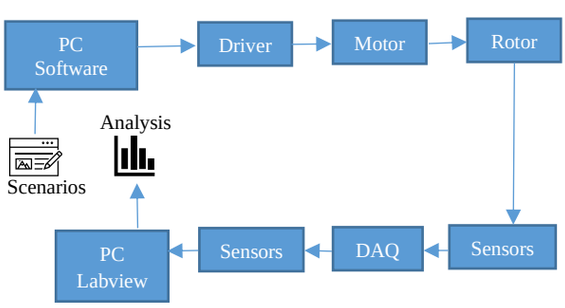

Figure 3 Diagram of data acquisition and control of induction motor speed in open loop
Source: Own elaboration

Below, the used instrumentation equipment for the development of this work is shown.

Figure 4 shows the first part of the instrumentation set equipment: the frequency inverter PowerFlex 525, the induction motor, mechanical transmission shaft, the current meter and oscilloscope.

Figure 4 shows the first part of the instrumentation set equipment: the frequency inverter PowerFlex 525, the induction motor, mechanical transmission shaft, the current meter and oscilloscope.

Figure 4 First part of instrumental set
Source: UNACAR mechatronics laboratory facilities

Figure 5 shows the second part of the instrumentation set equipment for data acquisition and signal processing (accelerometers, DAQ acquisition card, and data interface HMI).

Figure 5 Second part of instrumental set
Source: UNACAR mechatronics laboratory facilities

ISSN-2531-2189

The vibrations are obtained by means of a network of accelerometers, where the signals are processed by a DAQ and through a LabVIEW system engineering software, the signals are analyzed and the data obtained in the frequency domain are extracted, on the other hand, the currents of the induction motor in the oscilloscope are analyzed, where the data obtained are processed by means of mathematical software for engineering calculations.

To analyze the vertical vibration in detail, sensors A and B were placed on the bearing as shown in the following figure 6. Lateral vibrations were not considered in this analysis because the vertical magnitudes give more significant changes experimentally.

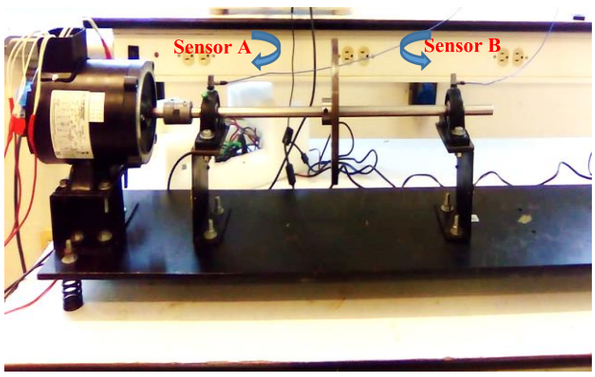

Figure 6 Location of accelerometers A and B on the bearing of rotodynamic system
Source: UNACAR mechatronics laboratory facilities

Experimental test

The results of the tests carried out on the rotodynamic system are acquired using two steel transmission bars, one of 0.60 meters and the other of 0.75 meters, which vibrate in a particular way at different speeds. The measurement of motor current disturbances due to the length of the steel transmission bar are post-processed using the Fourier Fast Transformation FFT that the oscilloscope itself has as mathematical tools, resulting in the same frequency spectrum as the methodology that uses accelerators, DAQ, software LabVIEW and PC. The advantage of using accelerometer is the more significant magnitudes relative to the FFT using motor currents.

Test 1

In the first test, a 0.60 m long transmission bar with balanced and unbalanced inertia disc is used. The frequency spectrum of the motor current processed with the mathematical tools of the oscilloscope and the frequency spectrum of the mechanical vibrations with accelerometers are measured with the oscilloscope and the LabVIEW software respectively. The results obtained are shown in Graphs 1 and 2, respectively.

Graphic 1 shows the Fourier spectra of the motor current, where two signals are observed; the first blue signal corresponds to the free-of-load or balanced condition, and the second orange signal, to the under-load or unbalanced condition, both at the same operating speed of 1725 rpm, which were measured by means of a tachometer.

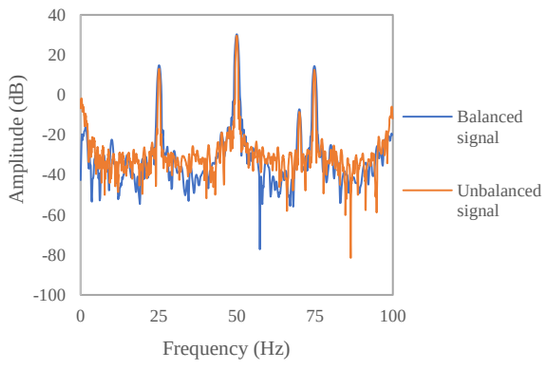

Graphic 1 Fourier spectra of motor currents first test
Source: Own elaboration

Graphic 2 shows the frequency spectra obtained from the mechanical vibrations of the system, where four signals are observed; the first signal in blue and the second in orange correspond to the accelerometers located on the bearing near and far from induction motor, respectively, in a free inertial or balanced load condition with an operating speed of 2,243 rpm. The third signal in gray and the fourth signal in yellow, correspond to the accelerometers located in the bearing near and far from the engine respectively, in condition under inertial load or unbalanced with an operating speed of 2,158 rpm.

ISSN-2531-2189

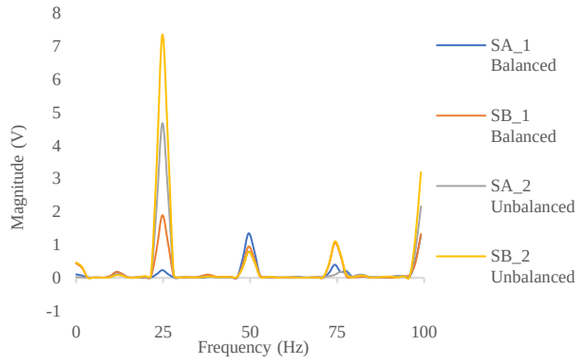

Graphic 2 Fourier spectra of the mechanical vibrations of the system first test
Source: Own elaboration

Test 2

In the second test, a 0.75 m long transmission bar with balanced and unbalanced inertia disc is used. like the first test. the frequency spectra are obtained using the measurement of motor current and mechanical vibrations. The results obtained are shown in Graphs 3 and 4, respectively. The results obtained are shown in Graphics 3 and 4, respectively.

Graphic 3 shows the Fourier spectra of the motor current, where two signals are observed; the first blue signal corresponds to the free-of-load or balanced condition, and the second orange signal, to the under-load or unbalanced condition, both at the same operating speed of 1,905 rpm.

In this test, like the first test, the change in magnitudes is almost negligible in balanced and unbalanced conditions, so it is not possible to adequately analyze different scenarios.

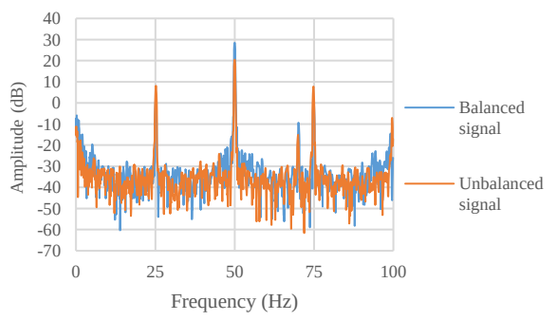

Graphic 3 Fourier spectrum of motor currents second test
Source: Own elaboration

Graphic 4 shows the frequency spectra obtained from the mechanical vibrations of the system, where four signals are observed; the first signal in blue and the second in orange correspond to the accelerometers located on the bearing near and far from induction motor, respectively, in a free inertial or balanced load condition with an operating speed of 1,550 rpm. The third gray signal and the fourth yellow signal correspond to the accelerometers located in the bearing near and far from induction motor, respectively, in free condition under inertial load or unbalanced with an operating speed of 1,905 rpm. In this test,

In this test, like the previous test in Graphic 2, it can be observed that the amplitude variation is much more significant than with the current sensors, so it is more convenient to use this type of instrumentation to determine the severity of the fault.

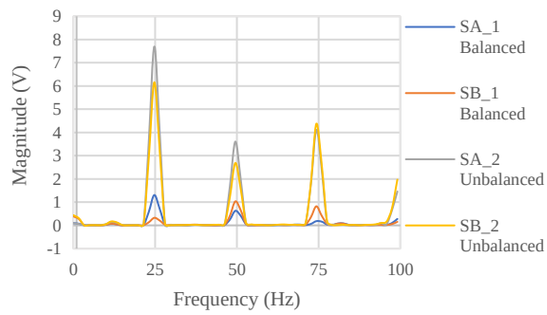

Graphic 4 Fourier spectrum of system vibrations second test
Source: Own elaboration

Discussion of results

In Graphics 1, 2, 3 and 4 it is observed that the central harmonics correspond to the electrical operating frequency of the motor, which is 50 Hz for Test 1 and 2. Here it is interesting to mention that system shaft speed is a function of operating frequency

On the other hand, the frequency of 25 Hz and 75 Hz for Test 1 and 2, are characteristic of the vibrations produced by the bearings of the pillow blocks. To corroborate these frequencies, it is necessary to know some internal parameters of the bearings, such as the shaft speed and dimensions of the diameters of the pellets, as reported in (Blanco-Ortega, 2010).

ISSN-2531-2189

Now, why do we have symmetrical side frequencies? if it is known that the two bearings used are the same. The answer is because vibrations always propagate within the same metal bearing diameter, but transversely. That is, the vibrations are doubled or tripled for each bearing with a different dimension.

The reason why could not operate at full speed of Test 1 and Test 2 could not be selected is because in an unbalanced system with a larger shaft, the vibrations increase to such a degree that the shaft becomes deformed.

Acknowledgements

The author gratefully acknowledges the support provided by both Consejo Nacional de Ciencia y Tecnología (CONACYT) and Universidad Autónoma del Carmen (UNACAR).

Conclusions

The results obtained from the motor currents and the mechanical vibrations of the rotodynamic system have very similar Fourier spectra.

The detection system can analyze the vibrations of the rotodynamic equipment, sensing a minimum load, but if the load is exceeded, the fault can be immediately propagated to induction motor.

The importance of the length of the shaft is fundamental in obtaining the samples, the greater the length of the shaft, the system experiences greater magnitudes of mechanical vibration and consequently a greater number of samples to be analyzed, Now, the shorter the shaft, the lower the vibration amplitude and the smaller the samples to analyze. So, the shorter the length of the transmission mechanical bar, the less mechanical vibration, and the fewer samples to analyze. This proposal can be improved by adding more sensors, to analyze not only the vertical vibrations but also the lateral vibrations

References

Ágoston, K. (2015). Fault detection of the electrical motors based on vibration analysis. *Procedia technology, 19*, 547-553.

Blanco-Ortega, A., Beltrán-Carbajal, F., Silva-Navarro, G., & Méndez-Azúa, H. (2010). Control de vibraciones en maquinaria rotatoria. *Revista Iberoamericana de Automática e Informática Industrial RIAI, 7*(4), 36-43.

de Abreu, J. P. G., & Emanuel, A. E. (October 2000). Induction motors loss of life due to voltage imbalance and harmonics: a preliminary study. *In Ninth International Conference on Harmonics and Quality of Power. Proceedings (Cat. No. 00EX441), Vol. 1*, (7-80) IEEE.

Donolo, P., Bossio, G., De Angelo, C., García, G., & Donolo, M. (2016). Voltage unbalance and harmonic distortion effects on induction motor power, torque and vibrations. *Electric power systems research, 140*, 866-873.

Gopinath, S. (2010, September). Study on electric motor mass unbalance based on vibration monitoring analysis technique. *In 2010 International Conference on Mechanical and Electrical Technology* , 539-542.

Hu, J. B. (2009). Proportional integral plus multi-frequency resonant current controller for grid-connected voltage source converter under imbalanced and distorted supply voltage conditions. *Journal of Zhejiang University-Science A,, 10*(10), 1532-1540.

Ioannides, M. G. (1995). A new approach for the prediction and identification of generated harmonics by induction generators in transient state. *IEEE transactions on energy conversion, 10*(1), 118-125.

Isermann, R. (2005). *Fault-diagnosis systems: an introduction from fault detection to fault tolerance.* Springer Science & Business Media.

Kersting, W. H. . (May 2000). Causes and effects of unbalanced voltages serving an induction motor. *In 2000 Rural Electric Power Conference. Papers Presented at the 44th Annual Conference (Cat. No. 00CH37071)*, (pp. B3-1). IEEE.

Khoobroo, A., Fahimi, B., & Lee, W. J. (November 2008). Effects of system harmonics and unbalanced voltages on electromagnetic performance of induction motors. *34th Annual Conference of IEEE Industrial Electronics In 2008*, 1173-1178.

Marín, E. P. (2012). *Elementos de medición y análisis de vibraciones en máquinas rotatorias.* Félix Varela.

Wang, Y. J. (January 2000). An analytical study on steady-state performance of an induction motor connected to unbalanced three-phase voltage. *In 2000 IEEE Power Engineering Society Winter Meeting. Conference Proceedings (Cat. No. 00CH37077), Vol.1*, (159-164) IEEE.

ISSN-2531-2189

[[Title in Times New Roman and Bold No. 14 in English and Spanish]

Surname (IN UPPERCASE), Name 1st Author†*, Surname (IN UPPERCASE), Name 1st Coauthor, Surname (IN UPPERCASE), Name 2nd Coauthor and Surname (IN UPPERCASE), Name 3rd Coauthor

Institutional Affiliation of Author including Dependency (No.10 Times New Roman and Italic)

International Identification of Science - Technology and Innovation

ID 1st Author: (ORC ID - Researcher ID Thomson, arXiv Author ID - PubMed Author ID - Open ID) and CVU 1st author: (Scholar-PNPC or SNI-CONACYT) (No.10 Times New Roman)

ID 1st Coauthor: (ORC ID - Researcher ID Thomson, arXiv Author ID - PubMed Author ID - Open ID) and CVU 1st coauthor: (Scholar or SNI) (No.10 Times New Roman)

ID 2nd Coauthor: (ORC ID - Researcher ID Thomson, arXiv Author ID - PubMed Author ID - Open ID) and CVU 2nd coauthor: (Scholar or SNI) (No.10 Times New Roman)

ID 3rd Coauthor: (ORC ID - Researcher ID Thomson, arXiv Author ID - PubMed Author ID - Open ID) and CVU 3rd coauthor: (Scholar or SNI) (No.10 Times New Roman)

(Report Submission Date: Month, Day, and Year); Accepted (Insert date of Acceptance: Use Only ECORFAN)

Abstract (In English, 150-200 words)

Objectives
Methodology
Contribution

Keywords (In English)

Indicate 3 keywords in Times New Roman and Bold No. 10

Abstract (In Spanish, 150-200 words)

Objectives
Methodology
Contribution

Keywords (In Spanish)

Indicate 3 keywords in Times New Roman and Bold No. 10

Citation: Surname (IN UPPERCASE), Name 1st Author, Surname (IN UPPERCASE), Name 1st Coauthor, Surname (IN UPPERCASE), Name 2nd Coauthor and Surname (IN UPPERCASE), Name 3rd Coauthor. Paper Title. Journal of Mechanical Engineering. Year 1-1: 1-11 [Times New Roman No.10]

* Correspondence to Author (example@example.org)
† Researcher contributing as first author.

Introduction

Text in Times New Roman No.12, single space.

General explanation of the subject and explain why it is important.

What is your added value with respect to other techniques?

Clearly focus each of its features

Clearly explain the problem to be solved and the central hypothesis.

Explanation of sections Article.

Development of headings and subheadings of the article with subsequent numbers

[Title No.12 in Times New Roman, single spaced and bold]

Products in development No.12 Times New Roman, single spaced.

Including graphs, figures and tables-Editable

In the article content any graphic, table and figure should be editable formats that can change size, type and number of letter, for the purposes of edition, these must be high quality, not pixelated and should be noticeable even reducing image scale.

[Indicating the title at the bottom with No.10 and Times New Roman Bold]

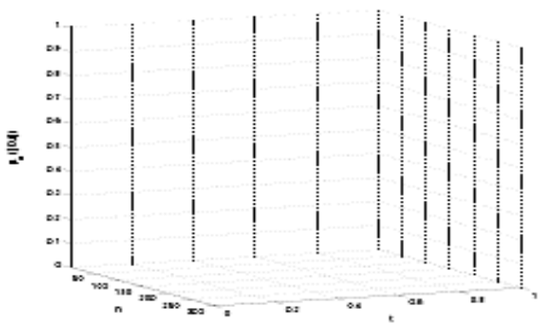

Graphic 1 Title and *Source (in italics)*

Should not be images-everything must be editable.

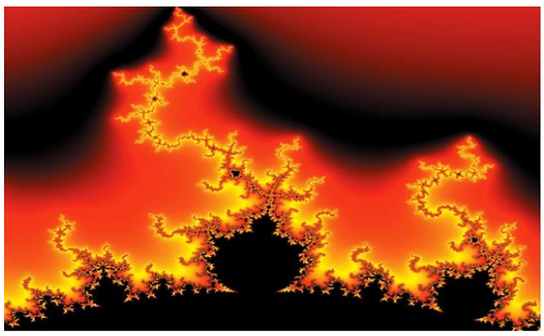

Figure 1 Title and *Source (in italics)*

Should not be images-everything must be editable.

Table 1 Title and *Source (in italics)*

Should not be images-everything must be editable.

Each article shall present separately in **3 folders**: a) Figures, b) Charts and c) Tables in .JPG format, indicating the number and sequential Bold Title.

For the use of equations, noted as follows:

$$Y_{ij} = \alpha + \sum_{h=1}^{r} \beta_h X_{hij} + u_j + e_{ij} \quad (1)$$

Must be editable and number aligned on the right side.

Methodology

Develop give the meaning of the variables in linear writing and important is the comparison of the used criteria.

Results

The results shall be by section of the article.

Annexes

Tables and adequate sources

Acknowledgment

Indicate if they were financed by any institution, University or company.

Conclusions

Explain clearly the results and possibilities of improvement.

ISSN 2531-2189

References

Use APA system. Should not be numbered, nor with bullets, however if necessary numbering will be because reference or mention is made somewhere in the Article.

Use Roman Alphabet, all references you have used must be in the Roman Alphabet, even if you have quoted an Article, book in any of the official languages of the United Nations (English, French, German, Chinese, Russian, Portuguese, Italian, Spanish, Arabic), you must write the reference in Roman script and not in any of the official languages.

Technical Specifications

Each article must submit your dates into a Word document (.docx):

Journal Name
Article title
Abstract
Keywords
Article sections, for example:

1. Introduction
2. Description of the method
3. Analysis from the regression demand curve
4. Results
5. Thanks
6. Conclusions
7. References

Author Name (s)
Email Correspondence to Author
References

Intellectual Property Requirements for editing:

-Authentic Signature in Color of Originality Format Author and Coauthors

-Authentic Signature in Color of the Acceptance Format of Author and Coauthors

ISSN 2531-2189

Reservation to Editorial Policy

Journal of Mechanical Engineering reserves the right to make editorial changes required to adapt the Articles to the Editorial Policy of the Journal. Once the Article is accepted in its final version, the Journal will send the author the proofs for review. ECORFAN® will only accept the correction of errata and errors or omissions arising from the editing process of the Journal, reserving in full the copyrights and content dissemination. No deletions, substitutions or additions that alter the formation of the Article will be accepted.

Code of Ethics - Good Practices and Declaration of Solution to Editorial Conflicts

Declaration of Originality and unpublished character of the Article, of Authors, on the obtaining of data and interpretation of results, Acknowledgments, Conflict of interests, Assignment of rights and Distribution.

The ECORFAN-Mexico, S.C. Management claims to Authors of Articles that its content must be original, unpublished and of Scientific, Technological and Innovation content to be submitted for evaluation.

The Authors signing the Article must be the same that have contributed to its conception, realization and development, as well as obtaining the data, interpreting the results, drafting and reviewing it. The Corresponding Author of the proposed Article will request the form that follows.

Article title:

– The sending of an Article to Journal of Mechanical Engineering emanates the commitment of the author not to submit it simultaneously to the consideration of other series publications for it must complement the Format of Originality for its Article, unless it is rejected by the Arbitration Committee, it may be withdrawn.

– None of the data presented in this article has been plagiarized or invented. The original data are clearly distinguished from those already published. And it is known of the test in PLAGSCAN if a level of plagiarism is detected Positive will not proceed to arbitrate.

– References are cited on which the information contained in the Article is based, as well as theories and data from other previously published Articles.

– The authors sign the Format of Authorization for their Article to be disseminated by means that ECORFAN-Mexico, S.C. In its Holding Spain considers pertinent for disclosure and diffusion of its Article its Rights of Work.

– Consent has been obtained from those who have contributed unpublished data obtained through verbal or written communication, and such communication and Authorship are adequately identified.

– The Author and Co-Authors who sign this work have participated in its planning, design and execution, as well as in the interpretation of the results. They also critically reviewed the paper, approved its final version and agreed with its publication.

– No signature responsible for the work has been omitted and the criteria of Scientific Authorization are satisfied.

–

The results of this Article have been interpreted objectively. Any results contrary to the point of view of those who sign are exposed and discussed in the Article.

Copyright and Access

The publication of this Article supposes the transfer of the copyright to ECORFAN-Mexico, SC in its Holding Spain for its Journal of Mechanical Engineering, which reserves the right to distribute on the Web the published version of the Article and the making available of the Article in This format supposes for its Authors the fulfilment of what is established in the Law of Science and Technology of the United Mexican States, regarding the obligation to allow access to the results of Scientific Research.

Article Title:

Name and Surnames of the Contact Author and the Coauthors	Signature
1.	
2.	
3.	
4.	

Principles of Ethics and Declaration of Solution to Editorial Conflicts

Editor Responsibilities

The Publisher undertakes to guarantee the confidentiality of the evaluation process, it may not disclose to the Arbitrators the identity of the Authors, nor may it reveal the identity of the Arbitrators at any time.

The Editor assumes the responsibility to properly inform the Author of the stage of the editorial process in which the text is sent, as well as the resolutions of Double-Blind Review.

The Editor should evaluate manuscripts and their intellectual content without distinction of race, gender, sexual orientation, religious beliefs, ethnicity, nationality, or the political philosophy of the Authors.

The Editor and his editing team of ECORFAN® Holdings will not disclose any information about Articles submitted to anyone other than the corresponding Author.

The Editor should make fair and impartial decisions and ensure a fair Double-Blind Review.

Responsibilities of the Editorial Board

The description of the peer review processes is made known by the Editorial Board in order that the Authors know what the evaluation criteria are and will always be willing to justify any controversy in the evaluation process. In case of Plagiarism Detection to the Article the Committee notifies the Authors for Violation to the Right of Scientific, Technological and Innovation Authorization.

Responsibilities of the Arbitration Committee

The Arbitrators undertake to notify about any unethical conduct by the Authors and to indicate all the information that may be reason to reject the publication of the Articles. In addition, they must undertake to keep confidential information related to the Articles they evaluate.

Any manuscript received for your arbitration must be treated as confidential, should not be displayed or discussed with other experts, except with the permission of the Editor.

The Arbitrators must be conducted objectively, any personal criticism of the Author is inappropriate.

The Arbitrators must express their points of view with clarity and with valid arguments that contribute to the Scientific, Technological and Innovation of the Author.

The Arbitrators should not evaluate manuscripts in which they have conflicts of interest and have been notified to the Editor before submitting the Article for Double-Blind Review.

Responsibilities of the Authors

Authors must guarantee that their articles are the product of their original work and that the data has been obtained ethically.

Authors must ensure that they have not been previously published or that they are not considered in another serial publication.

Authors must strictly follow the rules for the publication of Defined Articles by the Editorial Board.

The authors have requested that the text in all its forms be an unethical editorial behavior and is unacceptable, consequently, any manuscript that incurs in plagiarism is eliminated and not considered for publication.

Authors should cite publications that have been influential in the nature of the Article submitted to arbitration.

Information services

Indexation - Bases and Repositories

LATINDEX (Scientific Journals of Latin America, Spain and Portugal)
RESEARCH GATE (Germany)
GOOGLE SCHOLAR (Citation indices-Google)
REDIB (Ibero-American Network of Innovation and Scientific Knowledge- CSIC)
MENDELEY (Bibliographic References Manager)
HISPANA (Information and Bibliographic Orientation-Spain)
UNIVERSIA (University Library-Madrid)

Publishing Services

Citation and Index Identification H
Management of Originality Format and Authorization
Testing Article with PLAGSCAN
Article Evaluation
Certificate of Double-Blind Review
Article Edition
Web layout
Indexing and Repository
ArticleTranslation
Article Publication
Certificate of Article
Service Billing

Editorial Policy and Management

38 Matacerquillas, CP-28411. Moralzarzal –Madrid-España. Phones: +52 1 55 6159 2296, +52 1 55 1260 0355, +52 1 55 6034 9181; Email: contact@ecorfan.org www.ecorfan.org

Site Licences

03-2010-032610094200-01-For printed material, 03-2010-031613323600-01-For Electronic material,03-2010-032610105200-01-For Photographic material, 03-2010-032610115700-14-For the facts Compilation, 04-2010-031613323600-01-For its Web page, 19502-For the Iberoamerican and Caribbean Indexation, 20-281HB9- For its indexation in Latin-American in Social Sciences and Humanities,671-For its indexing in Electronic Scientific Journals Spanish and Latin-America,7045008-For its divulgation and edition in the Ministry of Education and Culture-Spain,25409-For its repository in the Biblioteca Universitaria-Madrid,16258-For its indexing in the Dialnet,20589-For its indexing in the edited Journals in the countries of Iberian-America and the Caribbean, 15048-For the international registration of Congress and Colloquiums. financingprograms@ecorfan.org

Management Offices

38 Matacerquillas, CP-28411. Moralzarzal –Madrid-España.

Journal of Mechanical Engineering

2531-2189
ISSN 2531-2189
www.ecorfan.org